



Contents lists available at ScienceDirect

NeuroImage

journal homepage: www.elsevier.com/locate/ynimg

Q1 Multimodal connectivity of motor learning-related dorsal premotor cortex

Q2 Robert M. Hardwick^a, Elise Lesage^b, Claudia R. Eickhoff^{c,d}, Mareike Clos^{c,e}, Peter Fox^f, Simon B. Eickhoff^{c,g,*}

4 ^a Department of Physical Medicine and Rehabilitation, Johns Hopkins University, USA

5 ^b Neuroimaging Research Branch, National Institutes of Drug Abuse, Baltimore, USA

6 ^c Institute for Neuroscience and Medicine (INM-1), Research Center Jülich, Germany

7 ^d Dept. of Psychiatry, Psychotherapy and Psychosomatics, RWTH Aachen University Hospital, Germany

8 ^e Department of Systems Neuroscience, University Medical Center Hamburg-Eppendorf, Germany

9 ^f University of Texas, USA

10 ^g Institute for Clinical Neuroscience and Medical Psychology, Heinrich-Heine-Universität, Germany

1 1 A R T I C L E I N F O

12 *Article history:*
13 Received 11 May 2015
14 Accepted 10 August 2015
15 Available online xxx

16 *Keywords:*
17 Motor learning
18 Functional connectivity
19 Resting state
20 Resting state functional connectivity
21 Meta-analytic connectivity modeling
22 Structural covariance

A B S T R A C T

The dorsal premotor cortex (dPMC) is a key region for motor learning and sensorimotor integration, yet we have 23 limited understanding of its functional interactions with other regions. Previous work have started to examine 24 functional connectivity in several brain areas using resting state functional connectivity (RSFC) and 25 meta-analytical connectivity modelling (MACM). More recently, structural covariance (SC) has also been 26 proposed as a technique that may also allow delineation of functional connectivity. Here, we applied 27 these three approaches to provide a comprehensive characterization of functional connectivity with a 28 seed in the left dPMC that a previous meta-analysis of functional neuroimaging studies has identified as 29 playing a key role in motor learning. Using data from two sources (the Rockland sample, containing resting 30 state data and anatomical scans from 132 participants, and the BrainMap database, which contains peak activation 31 foci from over 10,000 experiments), we conducted independent whole-brain functional connectivity mapping 32 analyses of a dPMC seed. RSFC and MACM revealed similar connectivity maps spanning prefrontal, premotor, 33 and parietal regions, while the SC map identified more widespread frontal regions. Analyses indicated a relatively 34 consistent pattern of functional connectivity between RSFC and MACM that was distinct from that identified by SC. 35 Notably, results indicate that the seed is functionally connected to areas involved in visuomotor control and 36 executive functions, suggesting that the dPMC acts as an interface between motor control and cognition. 37

© 2015 Published by Elsevier Inc.

38

39

41

43 Introduction

44 Converging evidence from single cell recordings, human neuroimaging, and neurostimulation paradigms indicate that the dorsal premotor cortex (dPMC) plays an important part in sensorimotor integration, response selection, and motor learning. Importantly, single-cell recording studies in non-human primates indicate the dPMC has limited ability to directly contribute to movement execution (Boudrias et al., 2010; Dum and Strick, 2005), but the region contains a high proportion of cells that respond to sensory cues, motor cues, or both (Weinrich and Wise, 1982). Thus, it has been suggested that the dPMC integrates sensory and motor information (Roland et al., 1980; Weinrich and Wise, 1982). Converging evidence from neuroimaging, neurostimulation, and neuropsychology indicates that the dorsal premotor cortex (dPMC) has a critical role in response selection (Bestmann et al., 2008; Halsband

et al., 1993; O'Shea et al., 2007; Rushworth et al., 2003; Zhang et al., 57 2011). There is also considerable evidence that the left dPMC in particular 58 plays a dominant role in visuomotor integration processes, while the right 59 dPMC is subservient (Bestmann et al., 2008; Hardwick et al., 2013; 60 Schubotz and von Cramon, 2002a, 2002b). Finally, a recent meta- 61 analysis of human neuroimaging studies has shown that the left dorsal 62 premotor cortex (dPMC) is consistently activated across a wide range of 63 motor learning paradigms, regardless of movement execution or the 64 hand being used (Hardwick et al., 2013). As of yet, however, the function- 65 al network of brain areas which interact with the left dPMC is relatively 66 unclear. Identifying the regions that functionally interact with the left 67 dPMC in humans would therefore further our understanding of how 68 this key node in the sensorimotor system contributes to response selec- 69 tion and motor learning. 70

Functional connectivity refers to the temporal coincidence of 71 spatially distant neurophysiological events (Friston, 1994). It is often 72 operationalized as a statistical relationship (usually a correlation) 73 between local neurobiological measures, and can therefore be considered 74 as a broad concept rather than one specific methodology. The advent of 75

* Corresponding author at: Institute of Neuroscience and Medicine, INM-1, Research Centre Jülich, Leo-Brandt-Straße, D-52428 Jülich, Germany.
E-mail address: s.eickhoff@fz-juelich.de (S.B. Eickhoff).

multiple connectivity analysis techniques in recent years has led to the possibility of assessing different aspects of functional connectivity. Resting state functional connectivity (RSFC) is driven by changes in BOLD activity in the absence of an experimental task (for a review, see Biswal, 2012). In seed-based correlation analysis, the time course of lower frequencies in the BOLD response extracted from a seed region are then compared with those of all voxels across the rest of the brain, with significant positive correlations implying functional connectivity. RSFC analyses offer the advantage of readily examining whole-brain connectivity without the constraint of a particular task. In comparison, meta-analytic connectivity modelling (MACM) provides a task-based approach to functional connectivity. MACM uses databases of activation peaks from neuroimaging studies to identify consistent co-activations across experiments (Eickhoff et al., 2010). While experiments are retrieved based on activation within a seed region, significant convergence of coordinates outside the seed reflects above-chance co-activation and hence implies functional connectivity. The large scale of the databases from which MACM analyses are derived provide a great strength to the technique (e.g. the BrainMap database contains >10,000 contrasts with >40,000 subjects). Finally, structural covariance (SC) uses the strength of grey matter volume correlations across the brain as an indicator of past co-activity. The underlying notion is that frequent activation leads to plastic changes in grey matter volume (Draganski et al., 2004), and frequently interacting (co-activating) regions thus co-vary in their grey matter densities (see, for example, Lerch et al., 2006). Thus, while SC uses a structural brain measure (grey matter volume), it crucially hinges upon functional interaction between brain regions following the principle of Hebbian plasticity (Hebb, 1949). Examining relationships in grey matter volume allows the assessment of consistent interaction between brain regions throughout development using a clearly defined measure, the physiological basis of which is clearly understood. In that context, it is important to also consider the different scales of integration (cf. Amunts et al., 2014) represented by these different methods: RSFC is a within-subject measure, MACM integrates across group activation findings, and SC is a cross-subject measure and cannot be determined on a single-subject basis. As previous studies indicate that functional connectivity is associated with correlated grey matter volumes (Seeley et al., 2009), we therefore regard it as a 'functional connectivity' measure (or, more precisely, a proxy for long-term functional connectivity patterns) for the purposes of this paper. While the degree to which SC can be used to infer functional networks has yet to be established (Clos et al., 2014), it provides a further method for investigating co-activity with the seed region.

Thus, RSFC, MACM, and SC are well-established techniques with the common goal of identifying brain networks interacting with the seed region, and may be used to assess 'functional connectivity' in the human brain. Each of these techniques probes 'functional connectivity' from a different angle, and has specific strengths and limitations. However, combining these tools provides a means to identify the core network of brain areas that consistently interacts with the chosen seed. To date, however, relatively few studies have directly compared results from these differing approaches. Recent papers combining the results of RSFC and MACM analyses have suggested good correspondence between the two methodologies (Bzdok et al., 2013; Clos et al., 2014; Hoffstaedter et al., 2013a; Jakobs et al., 2012; Müller et al., 2013; Rottschy et al., 2013). Results from comparisons of RSFC and SC also report correspondence between the two methodological approaches (Segall et al., 2012). While a combination of RSFC, MACM, and SC has previously been implemented as a method for parcellation (Kelly et al., 2012), only recently has a comparison of seed-based functional connectivity patterns arising from these three techniques been considered (Clos et al., 2014). As all three techniques use different methods to measure the same construct, comparing and contrasting their results provides a more comprehensive overview of 'functional connectivity'. In particular, a triangulation of their results would provide compelling evidence of the core functional connectivity with the seed region.

The importance of the left dPMC as a hub for sensorimotor integration makes it a prime candidate for examination using functional connectivity techniques. A recent meta-analysis has identified an area of the left dPMC that was the only region to consistently show increases in activity across a wide variety of motor learning paradigms (Hardwick et al., 2013). The essential role of this region in motor learning has not been recognized in previous models, which have primarily focused on the roles of the primary motor cortex and cerebellum in motor learning (e.g. Krakauer and Mazzoni, 2011). Identifying regions that functionally interact with this seed will therefore further our understanding of the network of areas that may contribute to motor learning. Here, we applied RSFC, MACM, and SC connectivity mapping techniques to provide a comprehensive overview of functional connectivity with this left dPMC seed region.

Material and methods

Seed region

A seed region in the left dPMC was defined based on the results of a recent meta-analysis of motor learning (Hardwick et al., 2013). This 35 mm³ region (peak MNI coordinates –32, –12, 60) survived a series of conjunctions across multiple subanalyses. These subanalyses strictly controlled for potentially confounding activations related to movement execution (i.e. considered only contrasts that compared movement during learning with execution of a similar baseline movement), and controlled for potential laterality effects due to the hand being used to perform the task. This area was therefore consistently activated across a wide variety of motor learning tasks. Data from two sources were utilized to assess functional connectivity with this seed region.

Data sources

The Rockland sample

The RSFC and SC analyses used data from the Nathan Kline Institute "Rockland" cohort (Nooner et al., 2012), available online via the International Neuroimaging Data sharing initiative (http://fcon_1000.projects.nitrc.org/indi/pro/nki.html). The sample used from this cohort consisted of 132 healthy subjects (78 M, 54 F), aged 18–85 years (mean ± SD: 42.3 ± 18.1 years). This sample was chosen as it provides a representative sample, and thus provides results that can be assumed to be representative of the general population.

The BrainMap database

The MACM analysis was conducted using the BrainMap database (Laird et al., 2011), using group average peak activation coordinates from neuroimaging studies examining within-subject contrasts in healthy individuals ("normal mapping", i.e., excluding any interventions such as pharmacological challenges, any longitudinal designs, and patient data, any between-group comparisons to test for differences, e.g. between genders). The BrainMap database was employed to identify task-based co-activation patterns across a large pool of neuroimaging experiments. At the time of processing, the database contained stereotaxic peak activation data including approximately 85,000 coordinates (foci) drawn from over 40,000 subjects across more than 10,000 experiments.

Functional connectivity analyses

Seed-based resting state functional connectivity

Images were acquired using a Siemens Tim Trio 3 T scanner using blood oxygen level-dependent (BOLD) contrast (260 whole-brain echo-planar imaging (EPI) volumes per subject, gradient-echo EPI pulse sequence, repetition time (TR) = 2.5 s, echo time (TE) = 30 ms, flip angle = 80°, in-plane resolution = 3 × 3 mm², 38 axial slices (3 mm thickness)). A seed-based RSFC analysis compares endogenous

fluctuations of BOLD activity in the seed region with that of all other voxels in the brain as a marker of functional connectivity under task-free conditions. Data were analyzed using SPM8 (Wellcome Trust Centre for Neuroimaging, London). The first four scans were discarded prior to analysis to allow for magnetic field saturation. The images were then corrected for movements by affine registration using a two-pass procedure. In the first step, images were aligned to the initial volumes, then subsequently to the mean of all volumes. The mean EPI image for each subject was then spatially normalized to the Montreal Neurological Institute (MNI) single-subject template (Holmes et al., 1998) using the unified segmentation approach (Ashburner and Friston, 2005). The resulting deformation was applied to the individual EPI volumes and images smoothed using a 5-mm full-width half-maximum (FWHM) Gaussian kernel. Spurious correlations for the time-series of each voxel were reduced by regressing out the nuisance variables of (1) the six motion parameters derived from image re-alignment; (2) their first derivatives; and (3) mean GM, WM, and CSF intensity. Nuisance variables were entered into the model as first- and second-order terms (see Satterthwaite et al., 2013 for an evaluation of this approach). In a final step, the data was band-pass filtered with cutoff frequencies of 0.01–0.08 Hz. Meaningful resting state correlations occur predominantly within this frequency band due to the low-pass filter-like effect of the BOLD signal (Fox and Raichle, 2007; Power et al., 2012).

The time course was extracted from the functionally defined left dPMC seed volume for each subject by computing the first eigenvariate of the time-series' of those voxels whose grey matter probability was above the median across all voxels in the ROI. Linear (Pearson) correlation coefficients were computed between this seed time series and the time series of all other grey matter voxels in the brain (Reetz et al., 2012; zu Eulenburg et al., 2012). The voxel-wise correlation coefficients were transformed into Fisher's z-scores and tested for consistency across subjects by a second-level ANOVA (including non-sphericity correction). This random effects analysis was family-wise error (FWE) corrected with a cluster level threshold of $p < 0.05$ (cluster forming threshold of $p < 0.001$ at voxel level).

Meta-analytic connectivity modelling

Meta-analytic connectivity modelling (MACM; Eickhoff et al., 2010; Robinson et al., 2010) assesses connectivity by determining brain areas that co-activate above chance with a seed region across multiple neuroimaging experiments. First, all experiments in the BrainMap database with at least one peak activation coordinate within the functionally defined left dPMC seed region were identified. Custom-written MATLAB scripts were then utilized to conduct an Activation Likelihood Estimation (ALE) meta-analysis (Eickhoff et al., 2009, 2012; Turkeltaub et al., 2002, 2012) across these in order to identify areas of converging activity across these experiments. The ALE algorithm empirically determines whether spatial convergence of foci between studies is greater than expected by chance. The highest convergence between studies evidently occurs within the seed (as all included experiments were selected based upon activity within the seed region). Significant convergence in areas beyond the seed is indicative of consistent co-activation (i.e. functional connectivity) with the seed region. Inference in the MACM analysis was conducted at $p < 0.05$ level (corrected for multiple comparisons using permutation testing, controlling cluster-level FWE at $p < 0.05$). While it is possible to restrict the sample of studies that are examined by MACM analyses, for instance, to examine only studies looking at motor control (cf. Hoffstaedter et al., 2013a,b), we here considered all studies within the BrainMap database. A pre-selection would introduce a bias not present in the RSFC and SC analyses. Selecting studies based on the location of their activations alone, however, provides a purely objective and data-driven approach to the MACM analysis. This allowed for unbiased comparisons between the results of the RSFC, MACM, and SC analyses.

Structural covariance

Structural covariance examines functional connectivity via correlations between regional grey matter properties such as volume or cortical thickness (Albaugh et al., 2013; He et al., 2007b; Lerch et al., 2006). Here, we used local volume as estimated by Voxel-based morphometry (VBM) on the anatomical T1 weighted MPRAGE scans from the 132 subjects in the Rockland sample to assess structural covariance. Images were acquired using a Siemens Tim Trio 3 T scanner as per the Rockland sample protocol (MPRAGE sequence, repetition time (TR) = 2.5 s, echo time (TE) 3.5 ms, flip angle = 8°, in-plane resolution = $1 \times 1 \text{ mm}^2$, 192 sagittal slices (1 mm thickness)). The anatomical scans were preprocessed using the VBM8 toolbox (dbm.neuro.uni-jena.de/vbm) in SPM8 using standard settings (DARTEL normalization, spatially adaptive non-linear means denoising, a Markov random field weighting of 0.15 and bias field modelling with a regularization term of 0.0001 and a 60 mm FWHM cutoff). These normalized grey matter segments, modulated only for the non-linear components of the deformations into standard space, were smoothed using an 8 mm FWHM Gaussian kernel (this normalization process accounts for differences in grey matter volumes between subjects). Statistical analysis was conducted in FSL1 with non-parametric statistics using the FSL 'permutest' function (Jenkinson et al., 2012; Smith et al., 2004). The volume for the functionally defined dPMC seed was computed in each subject by integrating the modulated voxel-wise grey matter probabilities under the seed cluster. This subject-specific local volume for the dPMC seed was used as the covariate of interest in the statistical group analysis. Statistical analysis was performed using the standard GLM implementation in FSL testing for each voxel whether the local volume of that particular voxel significantly covaried with the volume of the dPMC. Age was included in the statistical model as a variable of no interest. Inter-individual differences in brain volume were not included in the statistical model because they were already accounted for in the grey-matter probability maps (grey matter probability maps were modulated by non-linear components, and the analysed voxel values represent the absolute amount of tissue corrected for individual brain size). Significance was assessed at $p < 0.05$ as implemented by FSL (corrected for multiple comparisons using full permutation testing of TFCE images, threshold-free cluster enhancement; Smith and Nichols, 2009).

Difference analyses

Difference analyses identified which brain areas were most strongly associated with each functional connectivity mapping technique (Jakobs et al., 2012). These analyses were conducted in a multi-stage process. First, subtraction analyses were generated to compare the results from each functional connectivity analysis. The results of these subtraction analyses were combined in a conjunction on the minimum value, and masked by the original functional connectivity maps. The resulting image was thresholded to provide a map of regions with significantly higher connectivity values than in the counterpart analyses. For example, to generate a map of the areas that were more strongly associated with RSFC, the first step was to compute two subtraction analyses (RSFC minus MACM, RSFC minus SC). These difference analyses were combined in a conjunction, which identified the lowest value from each analysis for each voxel. The resulting voxels thus were significantly stronger connected to the seed in RSFC than in either of the two other techniques. Results were then masked by the original RSFC map (ensuring that regions most strongly associated with the RSFC technique would have to demonstrate significant connectivity during the original RSFC analysis). Finally, the resulting map was thresholded such that only voxels with a z-score greater than 1.96 (i.e. $p < 0.05$) were presented. The resulting map indicates which areas are more strongly associated with one of the examined connectivity mapping techniques compared to the other two methods.

327 *Conjunction analyses*

328 Conjunction analyses determined areas that were consistently
 329 activated across multiple brain connectivity approaches. Pairwise
 330 conjunctions were conducted between the three connectivity analyses
 331 in order to identify common results across the differing techniques. In
 332 addition, a combined analysis was performed across the results of
 333 RSFC, SC, and MACM. This combined conjunction thus identified areas
 334 with highly consistent functional connectivity to the left dPMC seed
 335 region. All conjunctions were computed by taking the minimum
 336 statistic (Jakobs et al., 2012; Nichols et al., 2005). Data from MACM
 337 were transformed from 2 mm³ MNI space to 1 mm³ for comparison
 338 with the RSFC and MACM data.

339 *Volume comparisons*

340 Previous studies have suggested that the volumes identified by RSFC,
 341 MACM, and SC show 'good convergence' (Bzdok et al., 2013; Clos et al.,
 342 2014; Hoffstaedter et al., 2013a; Jakobs et al., 2012; Müller et al., 2013;
 343 Rottschy et al., 2013). This has, however, been primarily examined
 344 through visual overlay of the identified maps, without further quantifi-
 345 cation. Here, we compared the volumes identified by each analysis, then
 346 quantified the volumes that were either uniquely identified by one
 347 analysis, or were identified by multiple analyses via conjunction.

348 *Volume-matched analyses*

349 Differences in the approaches employed by each of the analyses led
 350 to differences in the size of the total volumes of the brain that were
 351 identified as having functional connectivity with the motor learning-
 352 related seed region. A control analysis therefore aimed to determine
 353 whether the different functional connectivity mapping techniques
 354 examined identified broadly similar patterns of connectivity that
 355 differed mainly due to differences in statistical thresholding, or whether
 356 the different techniques identified truly divergent networks. The
 357 network with the smallest overall volume was identified (the MACM
 358 map, with a volume of 76,749 mm³). The thresholds of the RSFC and
 359 SC connectivity maps were then iteratively increased until the volumes
 360 they identified were approximately equal to that of the MACM network.
 361 Further volume comparison analyses were then conducted on the
 Q6 volume-matched maps (Fig. 1).

363 *Labelling*

364 Results were anatomically labelled according to their most probable
 365 macroanatomical and cytoarchitectonic locations using the SPM Anatomy

Toolbox (Eickhoff et al., 2005, 2007). Additional labels were derived from 366
 a functional meta-analysis of motor cortical regions (Mayka et al., 2006). 367
 Peak maxima of the reported coordinates are presented in 1 mm³ MNI 368
 space. Only regions with 100 cohesive voxels were reported. 369

Results 370*Main analyses* 371*Resting state functional connectivity* 372

The RSFC analysis (Fig. 2A) identified regions where the BOLD time 373
 course correlated with that in the left dPMC seed volume. This analysis 374
 revealed a distributed network that contains large clusters in frontal and 375
 parietal regions, and smaller clusters in the occipitotemporal cortex, 376
 striatum, and cerebellum. Connectivity with most regions was bilateral, 377
 but stronger in the left supratentorial regions and right cerebellar 378
 regions, consistent with its connectivity with left-lateralized seed. 379
 Specifically, a widespread frontal cluster spanned premotor regions 380
 including the pre-SMA and SMA, ventral and dorsal premotor cortex, 381
 and extended into the bilateral dorsolateral prefrontal cortex, left IFG 382
 and the left anterior insula. A second large bilateral parietal cluster 383
 spanned left inferior and superior parietal lobules, and the bilateral 384
 precuneus. In addition, connectivity was found with the mid-cingulate 385
 gyrus, bilateral fusiform gyrus, and bilateral ventral occipitotemporal 386
 cortex roughly corresponding with area V5. This analysis was the 387
 only one to identify striatal and cerebellar regions (see Table 1). 388
 Specifically, RSFC connectivity was found with the bilateral thalamus Q7 389
 and the bilateral dorsal striatum. Cerebellar connectivity was more 390
 pronounced in the right cerebellar hemisphere, with a large cluster 391
 spanning lobules HVI and HVII (Crus I and II), and a smaller cluster 392
 in lobule HVIII. In the left cerebellar hemisphere, smaller clusters 393
 were present in lobules HVII (Crus I and II) and HVIII. 394

Meta-analytical connectivity mapping 395

MACM (Fig. 2B) provided the most restricted network of all three 396
 connectivity mapping techniques examined, revealing a bilateral 397
 network of fairly localized premotor and posterior parietal cortical 398
 structures (see Table 2). Consistent task-based co-activation with the 399
 left dPMC seed region was identified in the contralateral dPMC, and 400
 bilateral vPMC, SMA, and IFG, extending into the anterior insula. Addi- 401
 tional connectivity was found in localized clusters in the left ventral 402
 occipitotemporal cortex, bilateral precuneus and intraparietal cortex, 403
 along with smaller clusters in the right angular gyrus and superior parietal 404
 lobule. The MACM analysis was unique in identifying connectivity with 405
 the left anterior insula. The MACM analysis did not reveal connectivity 406
 with subcortical regions. 407

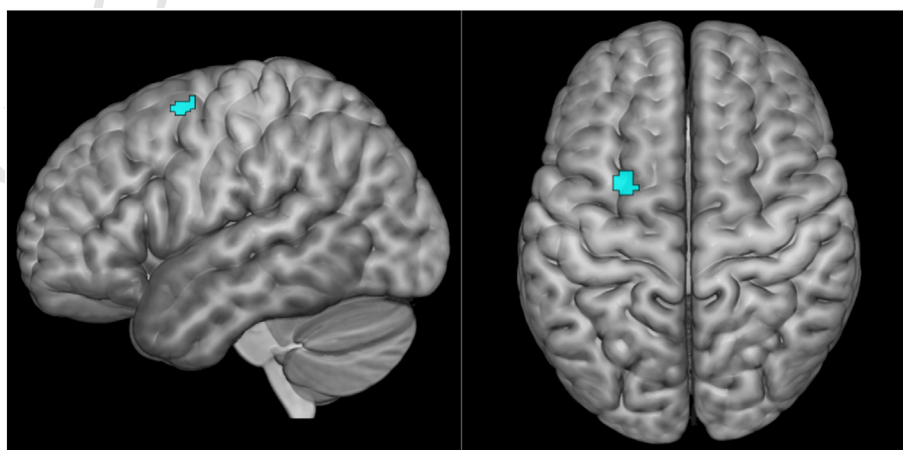


Fig. 1. The left dPMC seed region. A previous meta-analysis of motor learning (Hardwick et al., 2013) identified this seed as a key area for motor learning. The seed region was the sole area surviving multiple analyses that strictly controlled for both movement execution and hand use.

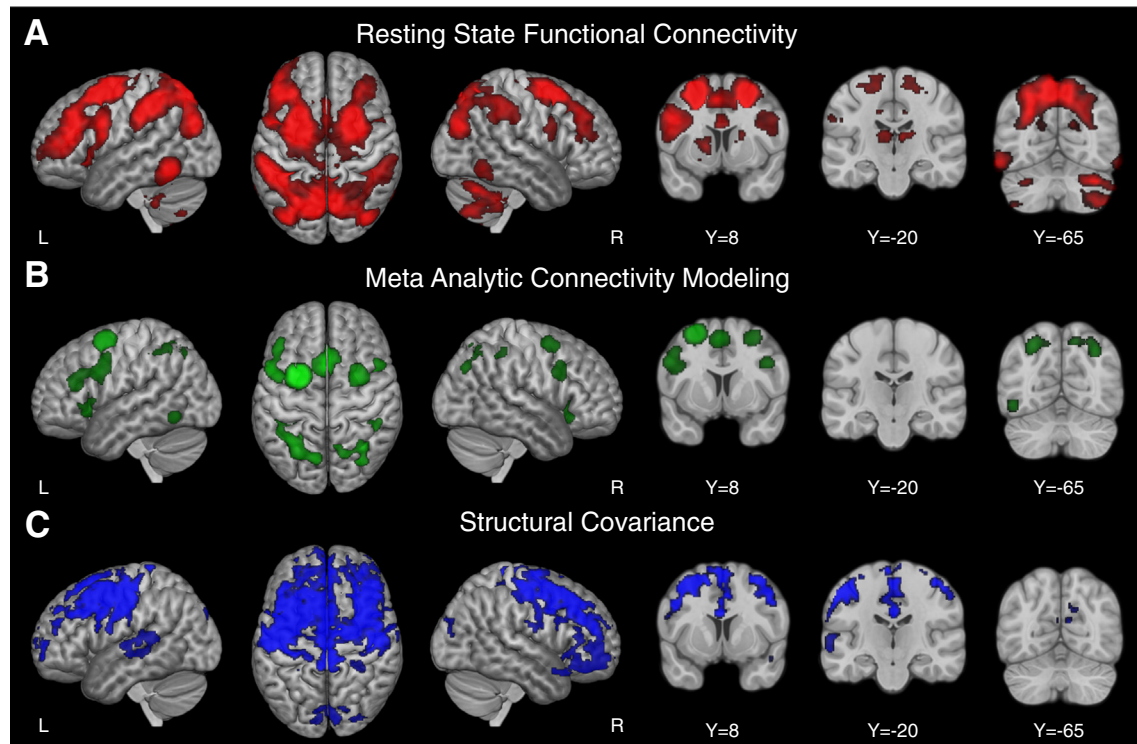


Fig. 2. Results of the connectivity analyses. (A) The resting state analysis (red) revealed the largest functional connectivity network, including frontal-premotor, and parietal cortex, as well as the thalamus, putamen, and cerebellar regions. (B) Meta-analytical connectivity modelling (green) gave relatively focal results with a bilateral network of premotor and parietal cortical structures. (C) The structural covariance analysis (blue) identified a large functional connectivity network, with widespread clusters, predominantly in prefrontal and motor/premotor areas.

Table 1
Resting state functional connectivity.

#	Vol (mm ³)	Macro	Cyto	t-score	MNI Coordinates		
					X	Y	Z
1	172,308	L dPMC R dPMC L SMA L vPMC L inferior frontal gyrus (p. triangularis) L putamen L thalamus R thalamus R vPMC	Area 44 Area 45	56.21 27.62 14.91 12.82 12.54 7.45 7.37 7.15 5.96	-26 26 -4 -46 -48 -16 -6 8 50	4 8 22 6 36 8 -14 -20 6	60 56 42 30 18 4 12 12 26
2	151,208	L precuneus L inferior parietal lobule L precuneus R precuneus L inferior parietal lobule L inferior parietal lobule L inferior parietal lobule L superior parietal lobule	SPL (7A) hIP2 SPL (7P) SPL (7P) IPC (PF) hIP2 hIP1 SPL (7P)	18.68 16.92 16.50 16.29 15.53 15.46 15.25 14.74	-6 -52 -8 8 -52 -38 -36 -16	-64 -42 -72 -70 -34 -48 -48 -74	54 48 54 52 44 50 48 54
3	24,072	R cerebellum R cerebellum R cerebellum R cerebellum	Lobule VIIa Crus I (Hem) Lobule VI (Hem) Lobule VIIa Crus II (Hem) Lobule VIIb (Hem)	12.31 11.71 8.78 8.69	36 30 38 30	-64 -62 -68 -70	-32 -32 -52 -50
4	12,071	L inferior temporal gyrus		14.95	-58	-58	-14
5	4,405	R inferior temporal gyrus		7.58	64	-58	-12
6	4,205	R cerebellum R cerebellum	Lobule IX (Hem) Lobule VIIIb (Hem)	9.67 4.60	14 12	-52 -62	-48 -62
7	4,063	L cerebellum L cerebellum	Lobule VIIa Crus I (Hem) Lobule VIIa Crus II (Hem)	7.51 3.24	-32 -48	-62 -48	-34 -50
8	3,529	L fusiform gyrus		9.51	-34	-38	-18
9	2,013	R cerebellum	Lobule IX (Hem)	7.99	-12	-52	-50
10	1,977	R fusiform gyrus		6.04	34	-34	-20
11	1,315	L cerebellum	Lobule VIIa Crus II (Hem) Lobule VIIb (Hem)	5.75 3.22	-38 -24	-70 -72	-54 -52

Table 2
Meta-analytical connectivity modelling.

	#	Vol (mm ³)	Macro	Cyto	z-score	MNI Coordinates		
						X	Y	Z
t2.5	1	22,522	L dPMC		8.57	-26	4	60
t2.6			L SMA	Area 6	7.89	-2	12	54
t2.7			R SMA		7.51	6	22	46
t2.8	2	12,497	L inferior parietal lobule	hIP3	7.30	-30	-56	48
t2.9			L precuneus	SPL (7P)	5.57	-12	-72	48
t2.10			L inferior parietal lobule	hIP2	4.26	-46	-36	44
t2.11	3	12,293	L inferior parietal lobule	Area 2	4.25	-44	-34	44
t2.12			L inferior parietal lobule	hIP1	3.56	-38	-44	44
t2.13			L vPMC	Area 44	6.27	-52	10	32
t2.14	4	6,813	L inferior frontal gyrus (p. triangularis)		5.26	-44	32	20
t2.15			L inferior frontal gyrus (p. triangularis)	Area 45	4.80	-46	28	28
t2.16			R angular gyrus		6.41	34	-62	44
t2.17	5	6,307	R middle occipital gyrus		5.51	32	-76	34
t2.18			R superior parietal lobule	SPL (7P)	4.56	16	-68	52
t2.19			R precuneus	SPL (7A)	4.16	8	-60	50
t2.20	6	5,707	L insula lobe		6.95	-34	22	-4
t2.21			L inferior frontal gyrus (p. triangularis)	Area 44	4.03	-48	16	4
t2.22			R dPMC		6.03	28	2	54
t2.23	7	4,101	R vPMC		4.99	48	14	30
t2.24			Right inferior frontal gyrus (p. orbitalis)		5.29	34	24	-10
t2.25			Right inferior frontal gyrus (p. orbitalis)					
t2.26	8	3,025	Right inferior parietal lobule	hIP2	4.56	42	-42	44
t2.27			Right inferior parietal lobule	IPC (PF)	3.75	48	-40	48
t2.28			Right inferior parietal lobule	IPC (PFt)	3.67	50	-38	50
t2.29	9	1,745	Right inferior parietal lobule					
t2.30			Right inferior parietal lobule					
t2.31			Right inferior parietal lobule					
t2.32	10	1,739	Left inferior temporal gyrus		5.43	-48	-62	-10

Structural covariance

The SC analysis (Fig. 2C) revealed areas where the grey matter volume correlates with the grey matter volume in the left dPMC seed region. This analysis yielded large areas spanning most of the frontal lobe, from the primary motor cortex to the orbitofrontal cortex. Smaller clusters were identified in the temporal and parietal lobes (see Table 3). The pattern was largely bilateral but stronger on the left, consistent with a left-lateralized seed. Frontal significant grey matter correlations were found

bilaterally with the dPMC, IFG, SMA, and primary sensory and motor cortex. Unique to the SC analysis, connectivity was also identified with the mid-cingulate cortex, left middle temporal gyrus, right temporal pole, bilateral cuneus, and occipital gyrus. Notably, no clusters were identified in the parietal cortex, or in any subcortical regions.

Difference analyses

Resting state functional connectivity > (meta-analytic connectivity modelling and structural covariance)

Consistent with the very robust pattern of activation revealed by the RSFC analysis, the pattern of regions more strongly associated with this analysis (Fig. 3A) is very similar to that identified in the main analysis (Fig. 2A). The clusters most strongly associated with RSFC spanned bilateral premotor and supplementary motor regions stretching into the dorsolateral prefrontal cortex and anterior insula, as well as large areas of bilateral precuneus, superior and inferior parietal lobules, fusiform gyrus, and ventral occipitotemporal cortex. As the cluster in the left thalamus, bilateral putamen, and bilateral cerebellar regions were only identified as having connectivity with the seed by the RSFC analysis, the same pattern of subcortical activity were evidently more strongly associated with RSFC than the other techniques examined. Thus, most regions identified by the RSFC analysis, were more strongly identified with this method than with either the structural covariance modelling or meta-analytic connectivity modelling methods.

Meta-analytic connectivity modelling > (resting state functional connectivity and structural covariance)

Areas in which MACM was stronger than RSFC and SC were relatively small in volume. These areas included the bilateral anterior insula, left dPMC (slightly dorsal from the seed region) and right vPMC, as well as small clusters in the left inferior occipital gyrus and the superior parietal lobule (see Fig. 3B). Of these regions, the right ventral prefrontal cortex and right anterior cingulate cortex were solely identified in the MACM analysis. In the parietal and occipital brain areas, RSFC and MACM overlapped substantially, but small clusters were more strongly present in the MACM.

Table 3
Structural covariance connectivity.

	#	Vol (mm ³)	Macro	Cyto	t-score	MNI Coordinates		
						X	Y	Z
t3.5	1	162,399	L dPMC		3.54	-47	9	32
t3.6			R dPMC		3.52	27	2	61
t3.7			R dPMC	Area 6	3.35	24	-12	63
t3.8			L SMA	Area 6	3.29	-1	-3	67
t3.9			R inferior frontal gyrus (p. triangularis)		3.24	48	36	27
t3.10	2	10,584	L inferior frontal gyrus (p. opercularis)		3.21	-43	21	33
t3.11			R middle cingulate		3.16	3	-9	35
t3.12			R cuneus	Area 18	2.29	6	-79	21
t3.13			L cuneus		2.11	3	-78	30
t3.14			L superior occipital gyrus	SPL (7P)	1.91	-9	-81	41
t3.15	3	4,569	L cuneus	Area 17	1.90	-3	-84	17
t3.16			L cuneus	Area 18	1.90	-1	-81	18
t3.17			L superior temporal gyrus		2.05	-57	-28	8
t3.18			L superior temporal gyrus	OP 4	2.00	-60	-19	6
t3.19			L superior temporal gyrus	TE 3	1.98	-61	-31	13
t3.20	4	1,190	L middle temporal gyrus		1.94	-66	-42	8
t3.21			R S1	Area 3b	1.75	30	-37	57
t3.22			R S1	Area 2	1.73	30	-42	57
t3.23	5	1,000	R superior occipital gyrus		1.69	25	-88	27
t3.24			R middle occipital gyrus		1.68	30	-87	24

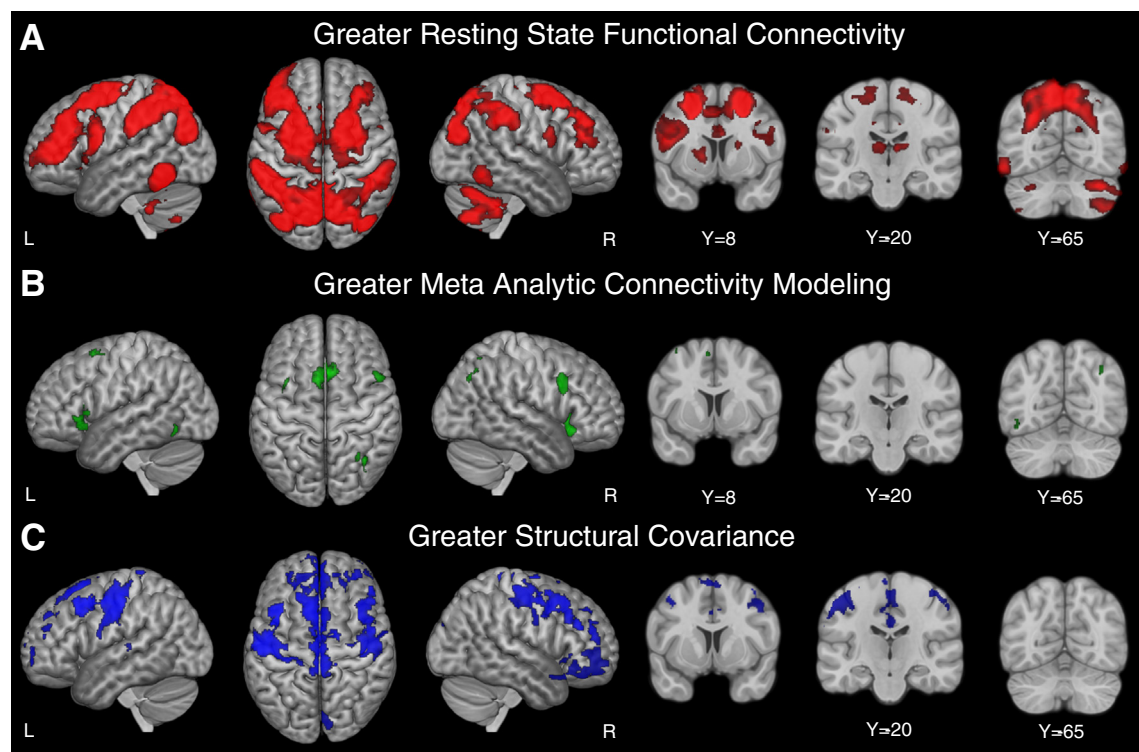


Fig. 3. Difference analyses presenting regions where one of the connectivity analyses provided significantly stronger scores than its counterparts. (A) Results were more strongly associated with RSFC, shown with red clusters. (B) Results were more strongly associated with MACM, shown with green clusters. (C) Results more strongly associated with SC, shown with blue clusters.

451 *Structural covariance > (resting state functional connectivity and*
 452 *meta-analytic connectivity modelling)*

453 Structural covariance yielded the strongest connectivity measures
 454 bilaterally across large areas of the frontal lobe and medial wall (see
 455 Fig. 3C). In the majority of these areas, there was a correlation of the
 456 grey matter volume between the dPMC seed and the grey matter
 457 volume in these regions, while the other two methods did not reveal
 458 significant connectivity with dPMC. Particularly striking are the robust
 459 bilateral clusters in the primary motor cortex, as well as the spread of
 460 the prefrontal cluster, which extended into the bilateral orbitofrontal
 461 gyrus and right frontal and temporal pole (see Fig. 3B). In addition,
 462 smaller clusters were found in the left superior temporal gyrus, left
 463 precuneus, and bilateral cuneus.

464 *Conjunction analyses*

465 Several conjunction analyses were carried out to shed light on
 466 regions commonly identified by the different connectivity analyses.
 467 The areas commonly identified in the RSFC and MACM analyses were
 468 fairly localized bilateral clusters in frontal and parietal lobes, with larger
 469 clusters ipsilateral to the left dPMC seed region (see Fig. 4A). These
 470 clusters were present in the right dorsal and ventral premotor cortex,
 471 supplementary motor cortex, and the left ventral premotor cortex
 472 extending into the dorsolateral prefrontal cortex and inferior frontal
 473 gyrus. Bilateral parietal clusters were present in the intraparietal sulcus
 474 and superior parietal lobule. The conjunction of analyses based on the
 475 Rockland sample (i.e. RSFC and SC analyses) revealed a widespread
 476 network spanning bilateral prefrontal and motor cortex, along with a
 477 few much smaller clusters in the superior parietal lobule and precuneus
 478 (see Fig. 4B). Only a small number of regions were commonly identified
 479 by SC and MACM analyses; these were in the left vPMC, SMA, and right
 480 dPMC (see Fig. 4C). Finally, the combined conjunction of all three
 481 connectivity analyses (i.e. RSFC, MACM, and SC; see Fig. 4D) was very

similar to the conjunction of the MACM and SC analyses. Specifically,
 these areas were the left vPMC, right dPMC, and the SMA.

Volume quantification

We quantified the volumes identified in each analysis to further
 investigate the differences and similarities between RSFC, MACM, and
 SC. We first quantified the total volumes identified by the RSFC,
 MACM, and SC analyses (Fig. 5A). RSFC identified the largest overall
 volume with functional connectivity with the seed (381,166 mm³).
 The RSFC network was more than double the size of the SC network
 (179,839 mm³), while the SC network was in turn more than double
 the size of the MACM network (76,749 mm³).

We then compared the convergence and divergence of the networks
 as examined in the conjunction analyses. Overlaying the RSFC and
 MACM networks (Fig. 5B) revealed that 81% were unique to the RSFC
 analysis, while only 3% was unique to the MACM analysis. The remaining
 16% of the overall volume was identified as surviving the conjunction of
 RSFC and MACM. Due to the disparity of their sizes, this meant that the
 majority of the volume identified in the MACM analysis was also identified
 by the RSFC analysis (see Venn diagram illustrating overlap; Fig. 5B).
 Pairwise comparisons indicated that 17% of the volume identified by
 RSFC analysis survived conjunction with the MACM map (see Fig. 5F),
 while 83% of the MACM map survived conjunction with the RSFC map
 (see Fig. 5G). Overlaying the RSFC and SC networks (Fig. 5C) revealed
 that 64% of the total volume identified was unique to RSFC, while 24%
 was unique to SC. Thus, 12% of the total volume identified in both
 analyses was shown to be commonly found in both techniques. Pairwise
 comparisons of these maps revealed that 16% of the RSFC map survived
 conjunction with the SC map (see Fig. 5H), while 34% of the SC map
 survived conjunction with the RSFC map (see Fig. 5I). Overlaying the
 MACM and SC networks (Fig. 5D) showed that 67% of the total network
 was unique to the SC analysis, while 23% was unique to the MACM

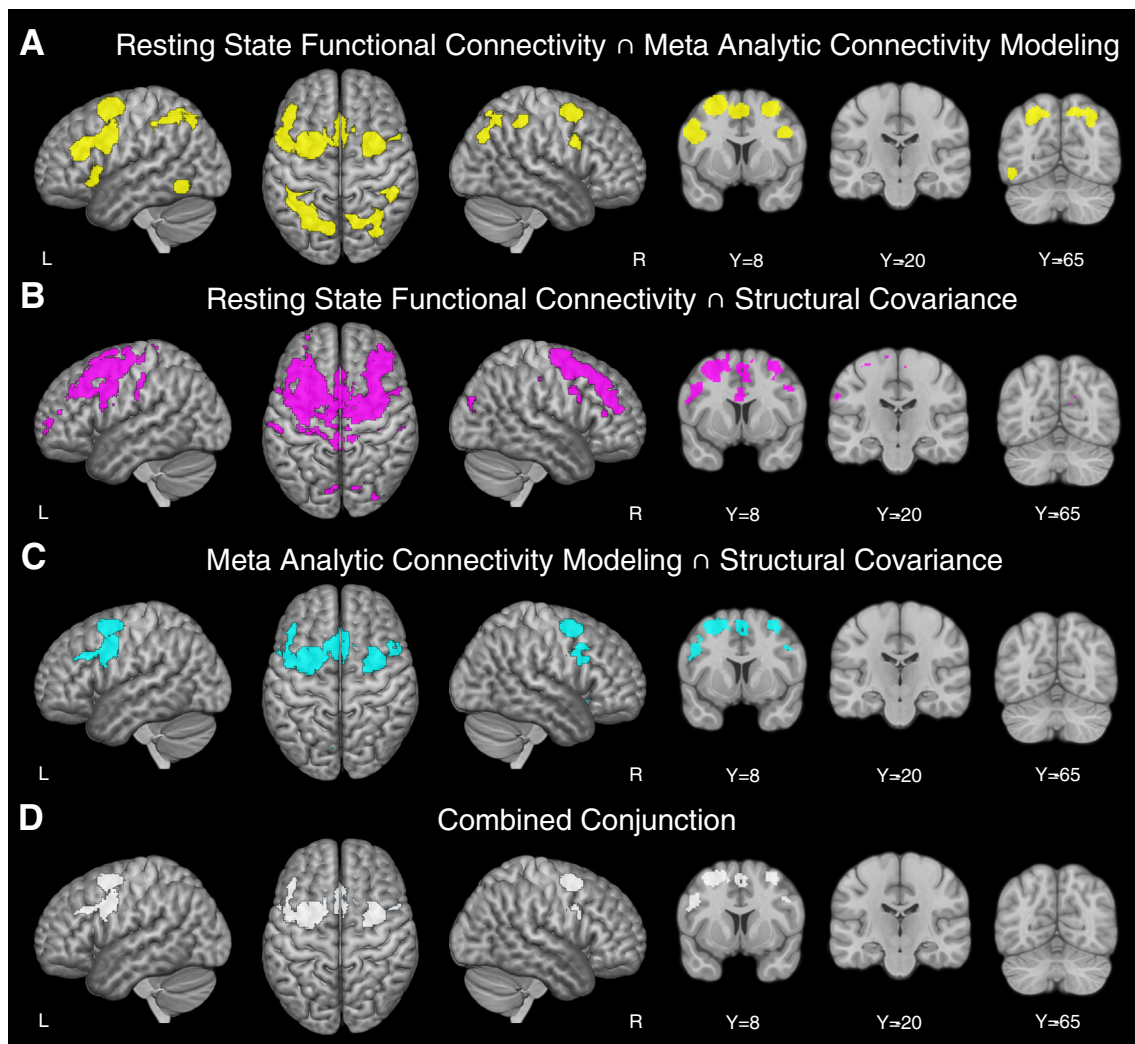


Fig. 4. Results of the conjunction analyses. (A) Conjunction of the RSFC and MACM analyses. (B) Conjunction of the RSFC and SC analyses. (C) Conjunction of the MACM and SC analyses. (D) A combined conjunction from all three analyses (RSFC, MACM, and SC), identifying a consistent 'core' network common to all connectivity mapping techniques considered.

analysis, and 10% was commonly identified in both maps. Pairwise comparisons showed that 29% of the MACM map survived conjunction with the SC map (see Fig. 5J), while 12% of the SC map survived conjunction with the MACM map 2(see Fig. 5K).

Finally, we considered the divergence and convergence between the RSFC, MACM, and SC maps in a combined analysis, overlaying all three functional connectivity maps. The majority of the volume identified by all three mapping techniques was unique to RSFC (54%) or the SC analysis (23%). A relatively small volume was identified only by MACM (2%). Conjunctions indicated that similar overall volumes were identified by both RSFC and MACM but not SC (8%), or RSFC and SC but not MACM (9%). In comparison, the volume identified by both MACM and SC but not RSFC was extremely small (1%). Considered relative to the total volume identified by all three analyses, only a small volume was identified in the combined conjunction of the RSFC, MACM, and SC analyses (4%; Fig. 6).

Volume-matched analyses

Results of the volume-matched control analysis were similar to those of the main analyses: RS and MACM identified relatively consistent networks of frontal, premotor, and parietal regions. In comparison, SC

revealed a network of areas more local to the seed, consisting mainly of prefrontal and premotor regions.

Volume-matched analyses: volume comparisons

Volume-matched analyses controlled for potential differences in the maps identified by each network arising from differences in the sizes of the volumes they identified. The volume-matched analysis iteratively increased the threshold of the RS and SC maps, reducing their volumes until they were approximately equal to that of the MACM analysis (see Fig. 7A). Overlaying the maps identified by the RSFC and MACM analyses showed that 24% of this volume was common to both analyses. A total of 39% of the volume of the volume-matched RSFC map survived conjunction with the MACM map, and (due to the volume matching approach), 39% of the MACM map survived conjunction with the RSFC map (see Fig. 7F,G). Overlaying the volume-matched RSFC analysis with the volume-matched SC analysis identified an 8% overlap (Fig. 7C). Of the volume-matched RSFC map, 15% survived conjunction with the volume-matched SC map, and vice versa (Fig. 7H,I). Overlaying the MACM map on the volume-matched SC map identified that 10% of the maps overlapped (Fig. 7D). For the MACM map, 18% survived conjunction with the volume-matched SC map, and vice versa (Fig. 7J,K). A combined

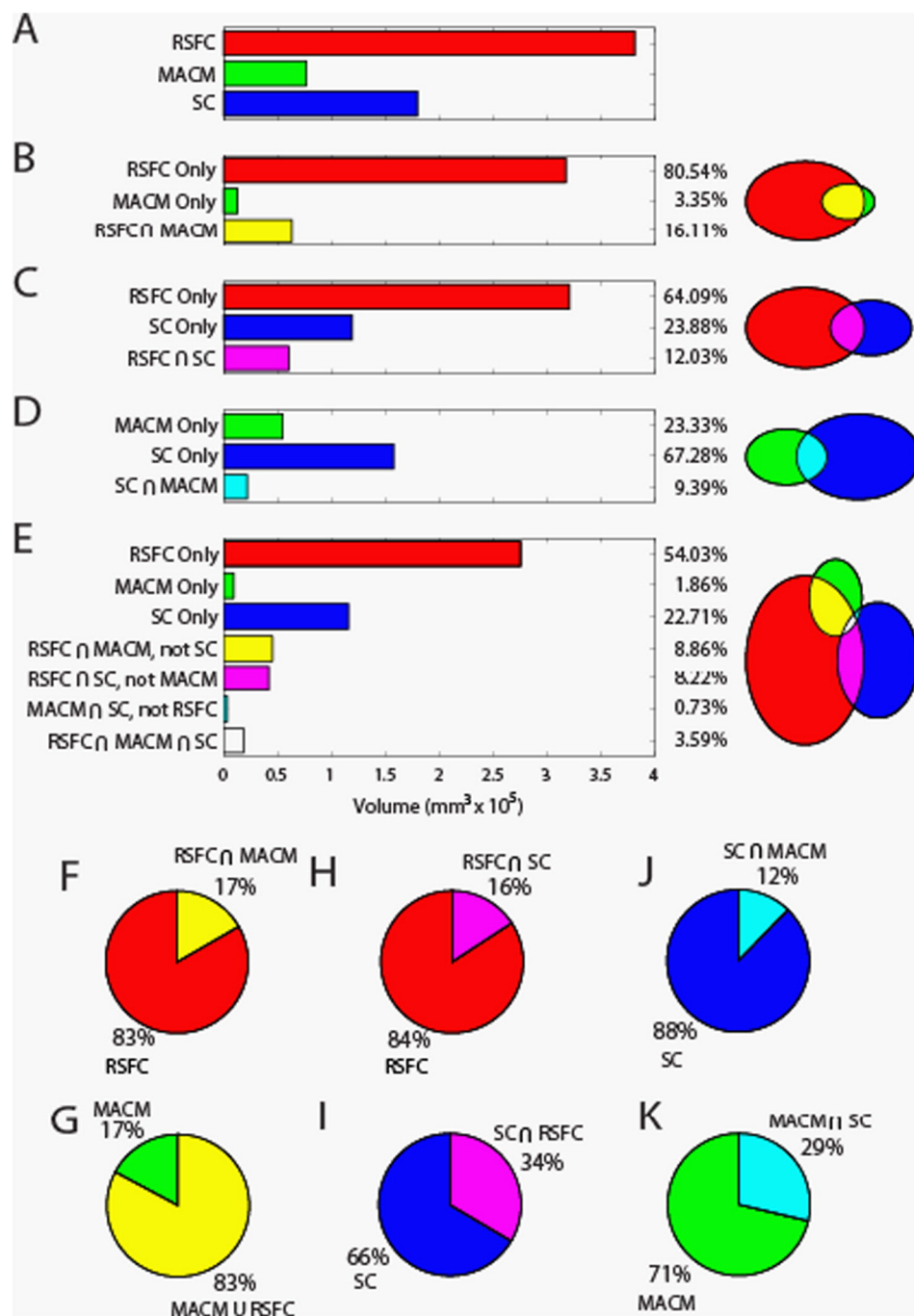


Fig. 5. Volume comparisons of the total volumes identified by the analyses, and their unique contributions and overlap. (A) Total volumes identified by the RSFC, MACM, and SC analyses. Further sections of the figure illustrate the overlap and disparity between total volumes identified by (B) the RSFC and MACM analyses, (C) the RSFC and SC analyses, (D) the SC and MACM analyses, and (E) the RSFC, MACM, and SC analyses. (F–K) pairwise comparisons illustrating the degree of overlap for each combination of analyses.

553 overlay analysis of all three maps also identified that the volume-matched
 554 SC analysis had the least overlap with other networks, consistent with the
 555 main analysis (Fig. 7E).

556 Discussion

557 The dPMC plays an essential role in integrating sensory and motor
 558 information (Roland et al., 1980; Weinrich and Wise, 1982), and the
 559 left dPMC in particular is consistently activated during a wide range of
 560 motor learning tasks (Hardwick et al., 2013). Despite the importance
 561 of the dPMC for sensorimotor integration and motor learning, there is
 562 limited understanding of the areas that functionally interact with it.
 563 The present study therefore examined regions that have functional

connectivity with a left dPMC region key to motor learning (Hardwick et al., 2013). We employed resting state functional connectivity (RSFC), meta-analytic connectivity mapping (MACM), and structural covariance (SC), comparing and combining their results to provide a comprehensive overview of connectivity with the seed. The maps resulting from the RSFC, MACM, and SC analyses identified networks of varying size and topography. Notably, the maps from the RSFC and MACM analyses were qualitatively similar, primarily spanning premotor and parietal regions. In comparison, the SC map identified predominantly frontal and temporal regions.

The differences between the maps for RSFC, MACM, and SC may be attributed to the methodological approaches employed by the three techniques. RSFC networks are based on “spontaneous”, task-free

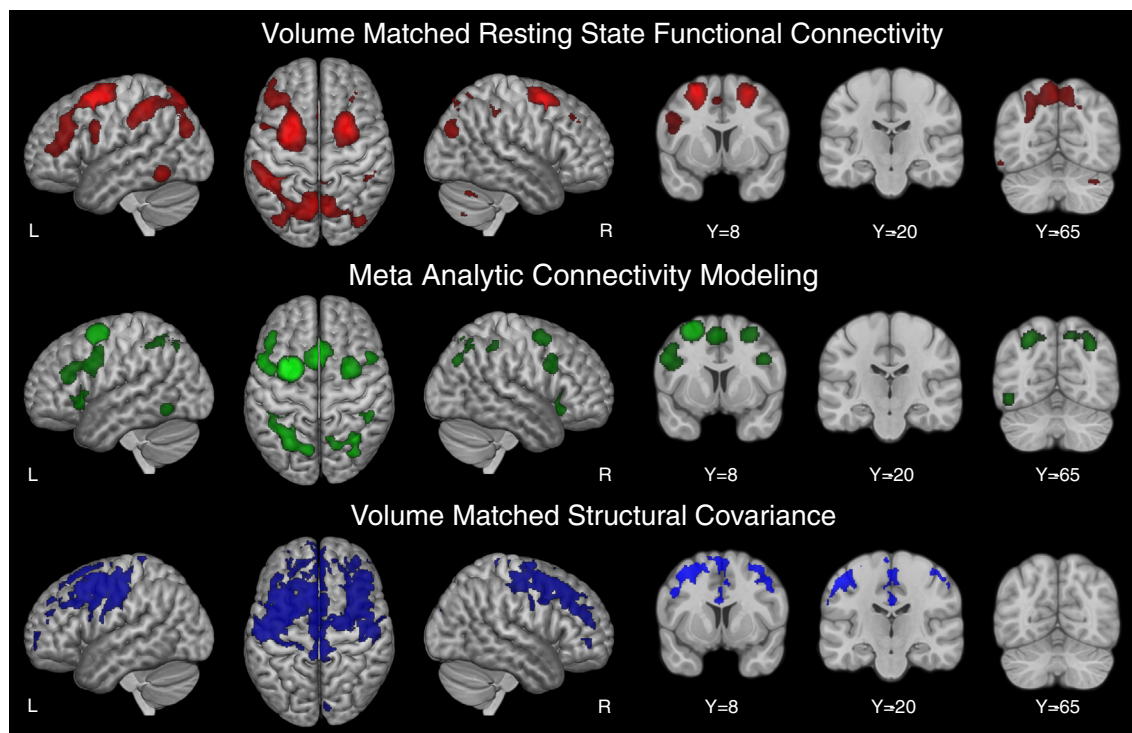


Fig. 6. Results of the conservatively thresholded RS and SC analyses in comparison to the results of the MACM analysis.

fluctuations in the BOLD signal, while MACM is based on the convergence of peak co-activity between task-based fMRI and PET experiments. Thus, the signals from RSFC and MACM are similar in that they both primarily encapsulate short term blood utilization in brain tissue. Note, however, that the RSFC analysis used only data from fMRI, while the MACM analysis amalgamated data from both fMRI and PET; these different modalities are known to influence activation profiles (Veltman et al., 2000), which could contribute to the differences seen between the RSFC and MACM analyses. In comparison, SC identifies correlations in grey matter volume between brain regions, and as such has less in common with RSFC and MACM. In addition, RSFC and MACM relate to comparatively short time spans, considering functional connectivity at rest (RSFC) or during the performance of specific tasks (MACM). The time span for SC is much longer, assessing differences in grey matter volume that have arisen throughout life thus far. An additional consideration is that the present study aimed to gain a comprehensive overview of functional connectivity with the dPMC seed region by examining *typical* applications of RSFC, MACM, and SC. As such, there are methodological differences between implementations, as is the case when each technique is used individually in the present literature. While it could be argued that standardizing these approaches may have reduced between-technique noise, such an approach would lead to questionable methodological choices; for instance, it is not feasible to assess VBM data (as used in SC) using cluster-level inference, which is standard in RSFC and MACM. Furthermore, attempting to rigidly match these procedures may artificially promote the homogeneity of the results. The present approach therefore allows further generalization of the results, allowing comparison of each individual analysis with those presently found in the literature.

A further consideration is that none of these techniques can perfectly capture functional connectivity, as each is subject to different sources of inherent noise. The spontaneous BOLD signal from which RSFC is derived is thought to be particularly susceptible to artefacts from preprocessing and physiological noise (Chang and Glover, 2009; Power et al., 2012). MACM is derived from peak coordinates from task-based fMRI and PET studies, and is thus constrained by the tasks possible to be performed in the scanner and the inherent spatial uncertainty of neuroimaging results (Eickhoff et al., 2009; Rottschy

et al., 2012). Finally, as well as representing experiences such as repeated practice of motor tasks (e.g. Gaser and Schlaug, 2003), differences in brain structure detected by SC are influenced by both environmental and hereditary factors throughout development (Alexander-Bloch et al., 2013).

To date, relatively few studies have compared results from all three of these techniques; most have compared RSFC with either MACM or SC (Bzdok et al., 2013; Jakobs et al., 2012; Rottschy et al., 2013; Segall et al., 2012). These investigations have generally reported that the two techniques they have examined provide qualitatively similar results. Here, we extended this work by quantifying the volumes identified by each analysis and their conjunctions, which further illustrated the relative similarities between the RSFC and MACM networks in comparison to the results of the SC analysis. Notably, RSFC and MACM are well-established methods for mapping functional connectivity (Biswal, 2012; Robinson et al., 2010), while the degree to which anatomical covariance networks as identified by SC are representative of functional connectivity is debatable (Clos et al., 2014). As a result, we first discuss the common functional connectivity network as identified by RSFC and MACM, then consider the added benefit and potential problems to consider when comparing their results to SC.

Areas with consistent functional connectivity: networks for motor learning identified by RSFC and MACM

As noted above, visualization of connectivity maps and volume quantifications indicated considerable convergence between the RSFC and MACM maps. The conjunction of these maps identified a consistent network of brain regions with functional connectivity to the motor learning-related seed region, including the right dPMC, bilateral ventral premotor cortex (vPMC), bilateral supplementary motor area (SMA), left dorsolateral prefrontal cortex (DLPFC), bilateral posterior parietal cortex, and left a V5/MT. This network is consistent with the role of the left dPMC as a central hub for sensorimotor integration and motor learning.

Interhemispheric dPMC interactions are well documented in motor control. Simple unilateral movements are typically associated with

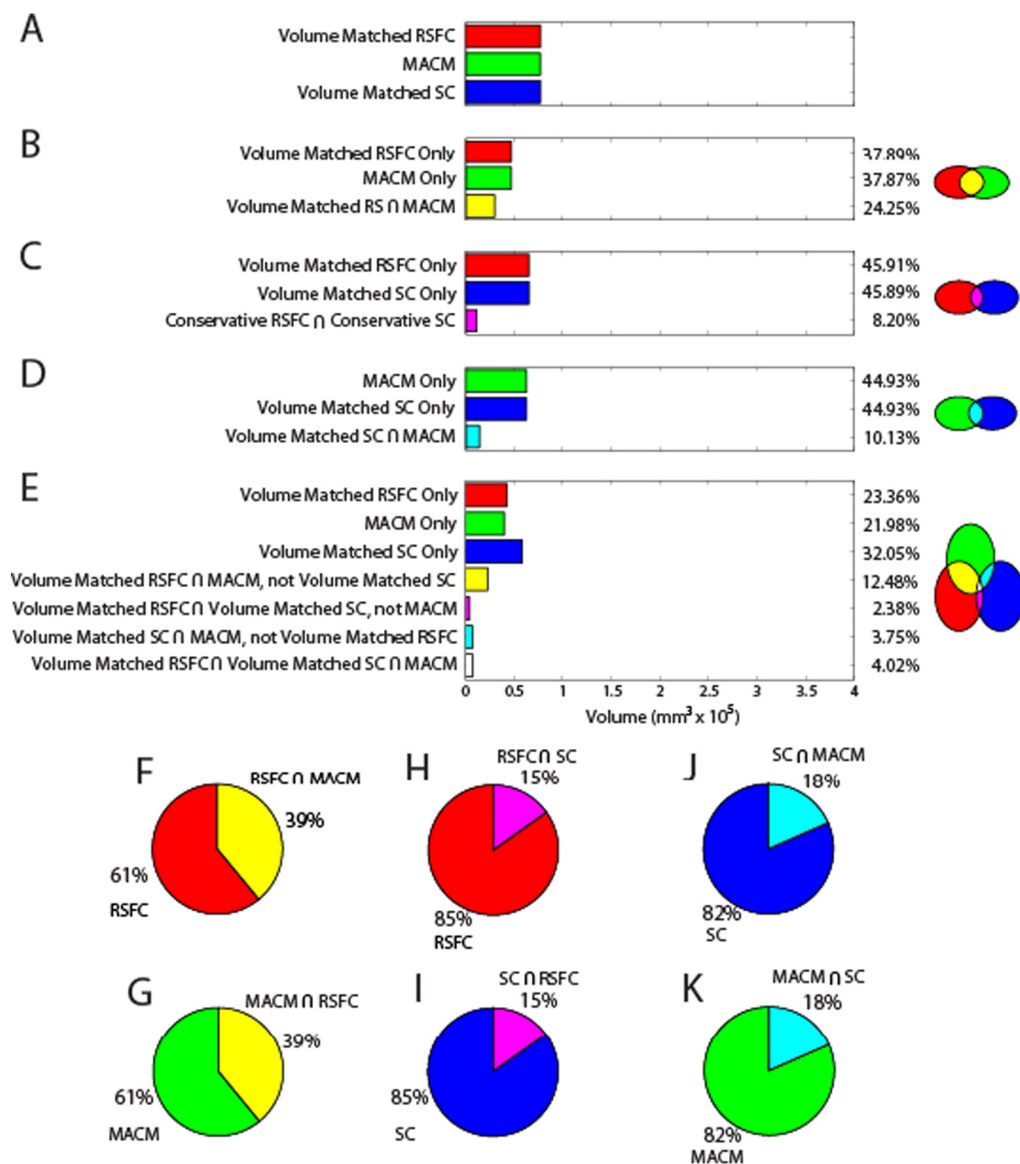


Fig. 7. Volume comparisons for the volume-matched analyses.

649 increases in bilateral dPMC activity in both non-human primates (Cisek
 650 et al., 2003; Tanji et al., 1988) and humans (Ward and Frackowiak,
 651 2003). The left dPMC is dominant in action selection (Bestmann et al.,
 652 2008), though the right dPMC can assume this role if the left dPMC is
 653 compromised (O'Shea et al., 2007). Studies of sequence learning have
 654 also identified increased right dPMC activity for the perceptual elements
 655 of sequences (Schubotz and von Cramon, 2002a, 2002b). The dPMC
 656 therefore appears to play a key role in volitional movement preparation,
 657 with the left dPMC being dominant for action selection and initiation,
 658 and the right dPMC playing a supportive role in acquisition and retrieval.
 659 Bihemispheric recruitment of the vPMC is also frequently observed in
 660 motor control (Binkofski et al., 1999; Davare et al., 2006; Ehrsson et al.,
 661 2000, 2001). The vPMC is specifically involved in the sensory guidance
 662 of hand movement (Binkofski et al., 1999), especially in hand shaping
 663 for precision grasp (Davare et al., 2006).

664 The SMA and left dPMC were also not only identified as having
 665 consistent connectivity across the RSFC, MACM, and SC analyses here
 666 but were also consistently linked with activation during motor learning
 667 in our previous meta-analysis (Hardwick et al., 2013). Moreover,
 668 consecutive days of motor training lead to parallel increases in their
 669 grey matter volumes (Hamzei et al., 2012). As both are active in motor

670 learning tasks that control for simple motor activity (Hardwick et al.,
 671 2013), they therefore appear to play a role in motor learning beyond
 672 movement execution itself. Both have been linked with movement
 673 sequences; the SMA being more closely associated with those that
 674 have been learned extensively (Wymbs and Grafton, 2013). The SMA
 675 has also classically been linked with the self-initiation of voluntary
 676 movements (Deecke and Kornhuber, 1978; Hoffstaedter et al., 2013b)
 677 and in switching between ongoing movement tasks (Nachev et al.,
 678 2008; Obeso et al., 2013). Increases in pre-SMA activity have frequently
 679 been associated with successful response inhibition (see Obeso et al.,
 680 2013; but also Criado and Boulinguez, 2013). The SMA therefore likely
 681 interacts with the dPMC in order to store movement sequences, and
 682 to initiate, modify, and possibly inhibit (or coordinate the inhibition
 683 of) actions.

684 Lesion studies in non-human primates indicate that the DLPFC plays
 685 an important role in rule-driven action selection (Wise and Murray,
 686 2000). Similarly, in humans, the DLPFC is associated with a role for
 687 rule representation within the working memory network (Nee et al.,
 688 2013). The DLPFC may therefore contribute to motor learning through
 689 providing declarative knowledge to be applied to motor output.
 690 Interestingly, interfering with the normal function of the DLPFC through

theta burst stimulation or cathodal transcranial direct current stimulation reduces declarative knowledge, but improves motor performance, presumably through placing an increased emphasis on implicit aspects of performance (Galea et al., 2010; Zhu et al., 2015). The DLPFC could therefore interact with the dPMC by providing declarative knowledge and relevant rules to guide motor output (see Wise and Murray, 2000).

The posterior parietal cortex receives multisensory inputs (see Grefkes and Fink, 2005), and is involved in weighting their evidence in order to produce appropriate motor output (Block et al., 2013). Notably, the regions demonstrating parietal connectivity in the conjunction of the RSFC and MACM maps included the superior parietal lobule (SPL), which was also found to be commonly activated in our recent meta-analysis of 70 motor learning experiments (Hardwick et al., 2013; see supplementary methods for comparison). The SPL has known physiological connectivity with the primate dPMC (Matelli et al., 1998), and their interaction is important for visuomotor control (Wise et al., 1997). Thus, multisensory input from the parietal lobe is thought to be processed to become motor output via an SPL-dPMC pathway (Cieslik et al., 2011; Johnson et al., 1993, 1996).

The inferior temporal cortex (ITC) is considered to be part of the ventral visual stream (Gross, 2008). ITC neurons respond only to visual stimuli (Gross et al., 1967, 1972), and are specialized for the recognition of shapes regardless of size, color, contrast, or location within the visual field (Schwartz et al., 1983; Rolls and Baylis, 1986). In humans, lesions of ITC lead to visual agnosia, characterized by an inability to recognize visual stimuli (Bauer, 2006). Association of a ventral stream area with motor control may seem surprising, as the dorsal visual stream is classically associated with movement (Goodale and Milner, 1992). However, functional connectivity with a region specialized in shape recognition is consistent with the essential role of the dPMC plays in producing motor responses to arbitrary visual stimuli (Wise and Murray, 2000).

Notable for a network involving motor control, the primary motor cortex (M1) was not identified as being functionally connected with the seed in the combined RSFC and MACM conjunction. M1 was also absent in the liberal analysis that removed thresholding from the MACM network (see supplementary results). This may seem surprising as there are known physiological connections between dPMC and M1 shown (Dum and Strick, 2005) and as dPMC excitability can affect M1 excitability in humans (Davare et al., 2009). However, RSFC connectivity does not always map onto anatomical connections (Di Martino et al., 2008; Kelly et al., 2010; Uddin et al., 2008; Vincent et al., 2007), and a previous study based on 1,000 subjects that parcellated the brain into RSFC networks did not show functional connectivity between M1 and premotor regions such as dPMC (Yeo et al., 2011). In addition, the absence of M1 from the MACM analysis may in large part be explained by the contrasts present in the BrainMap database. Most neuroimaging studies include controls for simple motor execution (see, for example, Daselaar et al., 2003; Inoue et al., 2000). Importantly, our previous finding that such contrasts remove M1 activation but still show dPMC activation (Hardwick et al., 2013) highlight the importance of the dPMC in higher-order motor processing.

Connectivity with the cerebellum was present in the RSFC analysis. In the right cerebellum, connectivity included regions associated with the lower hand representation in lobule HVIII (Thickbroom et al., 2003; Yeo et al., 2011), consistent with the importance of the cerebellum in motor control (Hardwick et al., 2013, 2014). Bilateral connectivity was also identified with lobules HVII (Crus I and II), which are involved in cognitive and linguistic processes (Lesage et al., 2012; Stoodley and Schmahmann, 2009), and are functionally connected to DLPFC and PPC (Buckner et al., 2011; O'Reilly et al., 2010). Given the importance of the cerebellum in motor control and learning, and the presence of cerebellar clusters of connectivity with the dPMC in the RSFC analysis, the absence of cerebellar clusters in the MACM analysis is perhaps surprising (though the MACM analysis did not identify the cerebellum as having functional connectivity with the dPMC, further analysis did identify multiple sub-threshold clusters of cerebellar connectivity; see supplementary results).

This difference can likely be attributed to the focus that many functional imaging studies place on imaging the cerebral cortex; the standard normalization process conducted in neuroimaging studies is not optimized for the cerebellum (Diedrichsen, 2006). Furthermore, inferior portions of the cerebellum are sometimes not covered by the field of view in many whole-brain fMRI studies, and when these regions are acquired, the default bounding box for normalization in certain software analysis packages do not include the entire cerebellum. This would lead to the absence of and greater variability in cerebellar coordinates than those in the cerebral cortex for many of the studies included in the BrainMap database, and may explain why the MACM analysis detected clusters in the cerebellum that did not survive thresholding.

Functional connectivity and structural covariance

As considered above, RSFC and MACM are previously established methods for identifying functional connectivity with a seed region, while the degree to which SC can determine functional connectivity is currently a subject of ongoing debate (Clos et al., 2014). Notably, while RSFC and MACM identified a similar network of frontal, premotor, and parietal regions, SC identified a network of mainly frontal regions that was more widespread than that revealed by the other two methods. This is consistent with findings from graph-theoretical SC analyses that report predominantly local connectivity (He et al., 2007a), and with data from seed-based SC analyses that identify regions largely limited to the lobe in which the seed is defined (Clos et al., 2014; Seeley et al., 2009; Zielinski et al., 2010). SC is thought to represent a combination of developmental coordination or synchronized maturation between brain areas (Alexander-Bloch et al., 2013). The SC network identified here is consistent with both of these properties; the prefrontal, premotor, and motor regions identified by SC are highly interconnected via anatomical fiber tracts (Bürgel et al., 1999, 2006; Carmichael and Price, 1995; Dum and Strick, 2005), and develop concurrently (Giedd et al., 1999).

The Rockland sample and the BrainMap database

The RSFC and SC analyses in the present study used whole-brain neuroimaging data from the Rockland sample. As data from the same subjects were used in both the RSFC and SC analyses, these analyses are therefore matched for factors such as age and gender. In contrast, the MACM analysis was based on data from the BrainMap database, which reports stereotaxic peak activation coordinates from published neuroimaging studies. Using peak coordinates leads to the loss of spatial information, but provides a pragmatic solution to the problems associated with sharing large datasets (current technical and practical limitations prevent the storage of whole-brain data from the 10,000+ neuroimaging studies included in the BrainMap database). Moreover, in spite of beginning data-sharing efforts, integrating published maxima coordinates are currently the only approach that allows summarization of the entire current literature. This loss of spatial information may account for the relatively small size of the volume identified by the MACM analysis in comparison to the RSFC and SC analyses. However, while these coordinates present a relatively sparse representation of the original activation maps they encapsulate, they also represent the most probable locations of activity from the activation maps they encapsulate, and thus provide a highly reliable source of data. Differences in sampling demographics may also influence the connectivity maps identified by each technique. The Rockland sample aims to produce a representative sample of individual subjects from the general population; in contrast, the BrainMap database stores average information from groups of subjects, and the papers from which this information is drawn do not always report demographic information in a uniform manner (e.g. some papers report mean subject ages, some report only age ranges). Similarly, it may be expected that the corpus of studies and contrast types contained within the BrainMap database could influence the results it provides; for example, as most

studies require participants to visual stimuli (vs. other modalities), there may be a bias toward finding activity in visual regions. However, sample bias effects appear unlikely given the high level of consistency between the MACM and RSFC maps (the latter of which by definition is not affected by task demands). Furthermore, it is notable that this study and others have identified similar results using RSFC and MACM (Bzdok et al., 2013; Clos et al., 2014; Hoffstaedter et al., 2013a; Jakobs et al., 2012; Müller et al., 2013; Rottschy et al., 2013). The consistency between results from RSFC and MACM illustrate that harnessing the large and varied sample from the BrainMap database can provide a powerful approach to functional connectivity.

830 Conclusions

831 Here, we employed multiple connectivity modelling techniques to
832 identify areas functionally interacting with a left dPMC region identified
833 as key for motor learning. RSFC, MACM, and SC offer different method-
834 ological and conceptual approaches to identifying functional connectivity
835 with a seed region, and were used here to provide a comprehensive
836 assessment of functional connectivity with the dPMC (cf. Clos et al.,
837 2014; Reid et al., 2015). Each approach identified networks with clear
838 differences in both their size and topography. However, further analyses
839 indicated that RSFC and MACM revealed a relatively consistent network
840 of prefrontal, premotor, and parietal regions, while the SC map consisted
841 mainly of widespread frontal regions. All techniques identified a consistent
842 'core' network of functional connectivity with the left vPMC, right
843 dPMC, and the SMA, all of which play important roles in the motor
844 control and learning (Hardwick et al., 2013). Most notably, conjunction
845 of the RSFC and MACM networks identified a consistent functional
846 network consisting of the bilateral dPMC, vPMC, SMA, and PPC, as well
847 as left hemisphere connectivity with the DLPFC and ITC. This network is
848 consistent with the established role of the dPMC in response selection,
849 suggesting that it supports motor learning by acting as an interface
850 between higher cognitive functions and visuomotor control.

851 Appendix A. Supplementary data

852 Supplementary data to this article can be found online at <http://dx.doi.org/10.1016/j.neuroimage.2015.08.024>.

854 References

- 855 Albaugh, M.D., Ducharme, S., Collins, D.L., Botteron, K.N., Althoff, R.R., Evans, A.C., Karama, S.,
856 Hudziak, J.J., 2013. Evidence for a cerebral cortical thickness network anti-correlated
857 with amygdalar volume in healthy youths: implications for the neural substrates of
858 emotion regulation. *Neuroimage* 71, 42–49. <http://dx.doi.org/10.1016/j.neuroimage.2012.12.071>.
- 859 Alexander-Bloch, A., Giedd, J.N., Bullmore, E., 2013. Imaging structural co-variance
860 between human brain regions. *Nat. Rev. Neurosci.* 14, 322–336. <http://dx.doi.org/10.1038/nrn3465>.
- 861 Amunts, K., Hawrylycz, M.J., Van Essen, D.C., Van Horn, J.D., Harel, N., Poline, J.-B., De
862 Martino, F., Bjaalie, J.G., Dehaene-Lambertz, G., Dehaene, S., Valdes-Sosa, P., Thirion,
863 B., Zilles, K., Hill, S.L., Abrams, M.B., Tass, P.A., Vanduffel, W., Evans, A.C., Eickhoff,
864 S.B., 2014. Interoperable atlases of the human brain. *Neuroimage* 99, 525–532.
865 <http://dx.doi.org/10.1016/j.neuroimage.2014.06.010>.
- 866 Ashburner, J., Friston, K.J., 2005. Unified segmentation. *Neuroimage* 26, 839–851. <http://dx.doi.org/10.1016/j.neuroimage.2005.02.018>.
- 867 **Q15** Bauer, R.M., 2006. The Agnosias. In: Snyder, P.J., Nussbaum, P.D., Robins, D.L. (Eds.), *Clinical*
871 *Neuropsychology: A Pocket Handbook for Assessment*. American Psychological
872 Association, Washington, DC, pp. 508–533.
- 873 Bestmann, S., Swayne, O., Blankenburg, F., Ruff, C.C., Haggard, P., Weiskopf, N.,
874 Josephs, O., Driver, J., Rothwell, J.C., Ward, N.S., 2008. Dorsal premotor cortex exerts
875 state-dependent causal influences on activity in contralateral primary motor and
876 dorsal premotor cortex. *Cereb. Cortex* 18, 1281–1291. <http://dx.doi.org/10.1093/cercor/bhm159>.
- 877 Binkofski, F., Buccino, G., Stephan, K.M., Rizzolatti, G., Seitz, R.J., Freund, H.J., 1999. A
878 parieto-premotor network for object manipulation: evidence from neuroimaging.
879 *Exp. Brain Res.* 128, 210–213.
- 880 Biswal, B.B., 2012. Resting state fMRI: a personal history. *Neuroimage* 62, 938–944. <http://dx.doi.org/10.1016/j.neuroimage.2012.01.090>.
- 881 Block, H., Bastian, A., Celnik, P., 2013. Virtual lesion of angular gyrus disrupts the relationship
882 between visuo-proprioceptive weighting and realignment. *J. Cogn. Neurosci.* 25,
883 636–648. http://dx.doi.org/10.1162/jocn_a_00340.

- Boudrias, M.-H., McPherson, R.L., Frost, S.B., Cheney, P.D., 2010. Output properties and
886 organization of the forelimb representation of motor areas on the lateral aspect of
887 the hemisphere in rhesus macaques. *Cereb. Cortex* 20, 169–186. <http://dx.doi.org/10.1093/cercor/bhp084>.
- Buckner, R.L., Krienen, F.M., Castellanos, A., Diaz, J.C., Yeo, B.T.T., 2011. The organization of
890 the human cerebellum estimated by intrinsic functional connectivity. *J. Neurophysiol.*
891 106, 2322–2345. <http://dx.doi.org/10.1152/jn.00339.2011>.
- Bürge, U., Schormann, T., Schleicher, A., Zilles, K., 1999. Mapping of histologically identified
893 long fiber tracts in human cerebral hemispheres to the MRI volume of a reference brain:
894 position and spatial variability of the optic radiation. *Neuroimage* 10, 489–499. <http://dx.doi.org/10.1006/nimg.1999.0497>.
- Bürge, U., Amunts, K., Hoemke, L., Mohlberg, H., Gilsbach, J.M., Zilles, K., 2006. White
897 matter fiber tracts of the human brain: three-dimensional mapping at microscopic
898 resolution, topography and intersubject variability. *Neuroimage* 29, 1092–1105.
899 <http://dx.doi.org/10.1016/j.neuroimage.2005.08.040>.
- Bzdok, D., Langner, R., Schilbach, L., Jakobs, O., Roski, C., Caspers, S., Laird, A.R., Fox, P.T.,
901 Zilles, K., Eickhoff, S.B., 2013. Characterization of the temporo-parietal junction by
902 combining data-driven parcellation, complementary connectivity analyses, and
903 functional decoding. *Neuroimage* 81, 381–392. <http://dx.doi.org/10.1016/j.neuroimage.2013.05.046>.
- Carmichael, S.T., Price, J.L., 1995. Sensory and premotor connections of the orbital and
906 medial prefrontal cortex of macaque monkeys. *J. Comp. Neurol.* 363, 642–664. <http://dx.doi.org/10.1002/cne.903630409>.
- Chang, C., Glover, G.H., 2009. Effects of model-based physiological noise correction on
909 default mode network anti-correlations and correlations. *Neuroimage* 47, 1448–1459. <http://dx.doi.org/10.1016/j.neuroimage.2009.05.012>.
- Cieslik, E.C., Zilles, K., Grefkes, C., Eickhoff, S.B., 2011. Dynamic interactions in the fronto-
912 parietal network during a manual stimulus-response compatibility task. *Neuroimage*
913 58, 860–869. <http://dx.doi.org/10.1016/j.neuroimage.2011.05.089>.
- Cisek, P., Crammond, D.J., Kalaska, J.F., 2003. Neural activity in primary motor and dorsal
915 premotor cortex in reaching tasks with the contralateral versus ipsilateral arm.
916 *J. Neurophysiol.* 89, 922–942. <http://dx.doi.org/10.1152/jn.00607.2002>.
- Clos, M., Rottschy, C., Laird, A.R., Fox, P.T., Eickhoff, S.B., 2014. Comparison of structural
918 covariance with functional connectivity approaches exemplified by an investigation
919 of the left anterior insula. *Neuroimage* 99, 269–280. <http://dx.doi.org/10.1016/j.neuroimage.2014.05.030>.
- Criaud, M., Boulinguez, P., 2013. Have we been asking the right questions when assessing
922 response inhibition in go/no-go tasks with fMRI? A meta-analysis and critical
923 review. *Neurosci. Biobehav. Rev.* 37, 11–23. <http://dx.doi.org/10.1016/j.neubiorev.2012.11.003>.
- Daselaar, S.M., Rombouts, S.A.R.B., Veltman, D.J., Raaijmakers, J.G.W., Jonker, C., 2003.
926 Similar network activated by young and old adults during the acquisition of a
927 motor sequence. *Neurobiol. Aging* 24, 1013–1019.
- Davare, M., Andres, M., Cosnard, G., Thonnard, J.-L., Olivier, E., 2006. Dissociating the role
929 of ventral and dorsal premotor cortex in precision grasping. *J. Neurosci.* 26,
930 2260–2268. <http://dx.doi.org/10.1523/JNEUROSCI.3386-05.2006>.
- Davare, M., Montague, K., Olivier, E., Rothwell, J.C., Lemon, R.N., 2009. Ventral premotor
932 primary motor cortical interactions during object-driven grasp in humans. *Cortex* 45,
933 1050–1057. <http://dx.doi.org/10.1016/j.cortex.2009.02.011>.
- Deecke, L., Kornhuber, H.H., 1978. An electrical sign of participation of the mesial "supple-
935 mentary" motor cortex in human voluntary finger movement. *Brain Res.* 159, 473–476.
- Di Martino, A., Scheres, A., Margulies, D.S., Kelly, A.M.C., Uddin, L.Q., Shehzad, Z., Biswal, B.,
937 Walters, J.R., Castellanos, F.X., Milham, M.P., 2008. Functional connectivity of human
938 striatum: a resting state fMRI study. *Cereb. Cortex* 18, 2735–2747. <http://dx.doi.org/10.1093/cercor/bhn041>.
- Draganski, B., Gaser, C., Busch, V., Schuierer, G., Bogdahn, U., May, A., 2004. Neuroplasticity:
941 changes in grey matter induced by training. *Nature* 427, 311–312. <http://dx.doi.org/10.1038/427311a>.
- Dum, R.P., Strick, P.L., 2005. Frontal lobe inputs to the digit representations of the motor
944 areas on the lateral surface of the hemisphere. *J. Neurosci.* 25, 1375–1386. <http://dx.doi.org/10.1523/JNEUROSCI.3902-04.2005>.
- Ehrsson, H.H., Fagergren, A., Jonsson, T., Westling, G., Johansson, R.S., Forssberg, H., 2000.
947 Cortical activity in precision- versus power-grip tasks: an fMRI study. *J. Neurophysiol.*
948 83, 528–536.
- Ehrsson, H.H., Fagergren, E., Forssberg, H., 2001. Differential fronto-parietal activation
950 depending on force used in a precision grip task: an fMRI study. *J. Neurophysiol.*
951 85, 2613–2623.
- Eickhoff, S.B., Stephan, K.E., Mohlberg, H., Grefkes, C., Fink, G.R., Amunts, K., Zilles, K., 2005.
953 A new SPM toolbox for combining probabilistic cytoarchitectonic maps and functional
954 imaging data. *Neuroimage* 25, 1325–1335. <http://dx.doi.org/10.1016/j.neuroimage.2004.12.034>.
- Eickhoff, S.B., Paus, T., Caspers, S., Grosbras, M.-H., Evans, A.C., Zilles, K., Amunts, K.,
957 2007. Assignment of functional activations to probabilistic cytoarchitectonic
958 areas revisited. *Neuroimage* 36, 511–521. <http://dx.doi.org/10.1016/j.neuroimage.2007.03.060>.
- Eickhoff, S.B., Laird, A.R., Grefkes, C., Wang, L.E., Zilles, K., Fox, P.T., 2009. Coordinate-based
961 activation likelihood estimation meta-analysis of neuroimaging data: a random-effects
962 approach based on empirical estimates of spatial uncertainty. *Hum. Brain Mapp.* 30,
963 2907–2926. <http://dx.doi.org/10.1002/hbm.20718>.
- Eickhoff, S.B., Jbabdi, S., Caspers, S., Laird, A.R., Fox, P.T., Zilles, K., Behrens, T.E.J., 2010.
965 Anatomical and functional connectivity of cytoarchitectonic areas within the
966 human parietal operculum. *J. Neurosci.* 30, 6409–6421. <http://dx.doi.org/10.1523/JNEUROSCI.5664-09.2010>.
- Eickhoff, S.B., Bzdok, D., Laird, A.R., Kurth, F., Fox, P.T., 2012. Activation likelihood estimation
969 meta-analysis revisited. *Neuroimage* 59, 2349–2361. <http://dx.doi.org/10.1016/j.neuroimage.2011.09.017>.

- Fox, M.D., Raichle, M.E., 2007. Spontaneous fluctuations in brain activity observed with functional magnetic resonance imaging. *Nat. Rev. Neurosci.* 8, 700–711. <http://dx.doi.org/10.1038/nrn2201>.
- Friston, K.J., 1994. Functional and effective connectivity in neuroimaging: a synthesis. *Hum. Brain Mapp.* 2, 56–78. <http://dx.doi.org/10.1002/hbm.460020107>.
- Galea, J.M., Albert, N.B., Ditye, T., Miall, R.C., 2010. Disruption of the dorsolateral prefrontal cortex facilitates the consolidation of procedural skills. *J. Cogn. Neurosci.* 22, 1158–1164. <http://dx.doi.org/10.1162/jocn.2009.21259>.
- Gaser, C., Schlaug, G., 2003. Brain structures differ between musicians and non-musicians. *J. Neurosci.* 23, 9240–9245.
- Giedd, J.N., Blumenthal, J., Jeffries, N.O., Castellanos, F.X., Liu, H., Zijdenbos, A., Paus, T., Evans, A.C., Rapoport, J.L., 1999. Brain development during childhood and adolescence: a longitudinal MRI study. *Nat. Neurosci.* 2, 861–863. <http://dx.doi.org/10.1038/13158>.
- Goodale, M.A., Milner, A.D., 1992. Separate visual pathways for perception and action. *Trends Neurosci.* 15, 20–25.
- Grefkes, C., Fink, G.R., 2005. The functional organization of the intraparietal sulcus in humans and monkeys. *J. Anat.* 207, 3–17. <http://dx.doi.org/10.1111/j.1469-7580.2005.00426.x>.
- Gross, C.G., Schiller, P.H., Wells, C., Gerstein, G.L., 1967. Single-unit activity in temporal association cortex of the monkey. *J. Neurophysiol.* 30, 833–843.
- Gross, C.G., Rocha-Miranda, C.E., Bender, D.B., 1972. Visual properties of neurons in inferotemporal cortex of the macaque. *J. Neurophysiol.* 35, 96–111.
- Halsband, U., Ito, N., Tanji, J., Freund, H.J., 1993. The role of premotor cortex and the supplementary motor area in the temporal control of movement in man. *Brain* 116 (Pt 1), 243–266.
- Hamzei, F., Glauche, V., Schwarzwald, R., May, A., 2012. Dynamic gray matter changes within cortex and striatum after short motor skill training are associated with their increased functional interaction. *Neuroimage* 59, 3364–3372. <http://dx.doi.org/10.1016/j.neuroimage.2011.10.089>.
- Hardwick, R.M., Rottschy, C., Miall, R.C., Eickhoff, S.B., 2013. A quantitative meta-analysis and review of motor learning in the human brain. *Neuroimage* 67, 283–297. <http://dx.doi.org/10.1016/j.neuroimage.2012.11.020>.
- Hardwick, R.M., Lesage, E., Miall, R.C., 2014. Cerebellar transcranial magnetic stimulation: the role of coil geometry and tissue depth. *Brain Stimul* <http://dx.doi.org/10.1016/j.brs.2014.04.009>.
- He, Y., Chen, Z.J., Evans, A.C., 2007a. Small-world anatomical networks in the human brain revealed by cortical thickness from MRI. *Cereb. Cortex* 17, 2407–2419. <http://dx.doi.org/10.1093/cercor/bhl149>.
- He, Y., Wang, L., Zang, Y., Tian, L., Zhang, X., Li, K., Jiang, T., 2007b. Regional coherence changes in the early stages of Alzheimer's disease: a combined structural and resting-state functional MRI study. *Neuroimage* 35, 488–500. <http://dx.doi.org/10.1016/j.neuroimage.2006.11.042>.
- Hoffstaedter, F., Grefkes, C., Caspers, S., Roski, C., Palomero-Gallagher, N., Laird, A.R., Fox, P.T., Eickhoff, S.B., 2013a. The role of anterior midcingulate cortex in cognitive motor control: evidence from functional connectivity analyses. *Hum. Brain Mapp.* <http://dx.doi.org/10.1002/hbm.22363>.
- Hoffstaedter, F., Grefkes, C., Zilles, K., Eickhoff, S.B., 2013b. The “what” and “when” of self-initiated movements. *Cereb. Cortex* 23, 520–530. <http://dx.doi.org/10.1093/cercor/bhr391>.
- Holmes, C.J., Hoge, R., Collins, L., Woods, R., Toga, A.W., Evans, A.C., 1998. Enhancement of MR images using registration for signal averaging. *J. Comput. Assist. Tomogr.* 22, 324–333.
- Inoue, K., Kawashima, R., Satoh, K., Kinomura, S., Sugiura, M., Goto, R., Ito, M., Fukuda, H., 2000. A PET study of visuospatial learning under optical rotation. *Neuroimage* 11, 505–516. <http://dx.doi.org/10.1006/nimg.2000.0554>.
- Jakobs, O., Langner, R., Caspers, S., Roski, C., Cieslik, E.C., Zilles, K., Laird, A.R., Fox, P.T., Eickhoff, S.B., 2012. Across-study and within-subject functional connectivity of a right temporo-parietal junction subregion involved in stimulus-context integration. *Neuroimage* 60, 2389–2398. <http://dx.doi.org/10.1016/j.neuroimage.2012.02.037>.
- Jenkinson, M., Beckmann, C.F., Behrens, T.E.J., Woolrich, M.W., Smith, S.M., 2012. FSL. *Neuroimage* 62, 782–790. <http://dx.doi.org/10.1016/j.neuroimage.2011.09.015>.
- Johnson, P.B., Ferraina, S., Caminiti, R., 1993. Cortical networks for visual reaching. *Exp. Brain Res.* 97, 361–365.
- Johnson, P.B., Ferraina, S., Bianchi, L., Caminiti, R., 1996. Cortical networks for visual reaching: physiological and anatomical organization of frontal and parietal lobe arm regions. *Cereb. Cortex* 6, 102–119.
- Kelly, C., Uddin, L.Q., Shehzad, Z., Margulies, D.S., Castellanos, F.X., Milham, M.P., Petrides, M., 2010. Broca's region: linking human brain functional connectivity data and non-human primate tracing anatomy studies. *Eur. J. Neurosci.* 32, 383–398. <http://dx.doi.org/10.1111/j.1469-9568.2010.07279.x>.
- Kelly, C., Toro, R., Di Martino, A., Cox, C.L., Bellec, P., Castellanos, F.X., Milham, M.P., 2012. A convergent functional architecture of the insula emerges across imaging modalities. *Neuroimage* 61, 1129–1142. <http://dx.doi.org/10.1016/j.neuroimage.2012.03.021>.
- Laird, A.R., Eickhoff, S.B., Fox, P.M., Uecker, A.M., Ray, K.L., Saenz, J.J., McKay, D.R., Bzdok, D., Laird, R.W., Robinson, J.L., Turner, J.A., Turkeltaub, P.E., Lancaster, J.L., Fox, P.T., 2011. The BrainMap strategy for standardization, sharing, and meta-analysis of neuroimaging data. *BMC Res. Notes* 4, 349. <http://dx.doi.org/10.1186/1756-0500-4-349>.
- Lerch, J.P., Worsley, K., Shaw, W.P., Greenstein, D.K., Lenroot, R.K., Giedd, J., Evans, A.C., 2006. Mapping anatomical correlations across cerebral cortex (MACACC) using cortical thickness from MRI. *Neuroimage* 31, 993–1003. <http://dx.doi.org/10.1016/j.neuroimage.2006.01.042>.
- Lesage, E., Morgan, B.E., Olson, A.C., Meyer, A.S., Miall, R.C., 2012. Cerebellar rTMS disrupts predictive language processing. *Curr. Biol.* 22, R794–R795. <http://dx.doi.org/10.1016/j.cub.2012.07.006>.
- Matelli, M., Govoni, P., Galletti, C., Kutz, D.F., Luppino, G., 1998. Superior area 6 afferents from the superior parietal lobule in the macaque monkey. *J. Comp. Neurol.* 402, 327–352.
- Mayka, M.A., Corcos, D.M., Leurgans, S.E., Vaillancourt, D.E., 2006. Three-dimensional locations and boundaries of motor and premotor cortices as defined by functional brain imaging: a meta-analysis. *Neuroimage* 31, 1453–1474. <http://dx.doi.org/10.1016/j.neuroimage.2006.02.004>.
- Müller, V.I., Cieslik, E.C., Laird, A.R., Fox, P.T., Eickhoff, S.B., 2013. Dysregulated left inferior parietal activity in schizophrenia and depression: functional connectivity and characterization. *Front. Hum. Neurosci.* 7, 268. <http://dx.doi.org/10.3389/fnhum.2013.00268>.
- Nachev, P., Kennard, C., Husain, M., 2008. Functional role of the supplementary and pre-supplementary motor areas. *Nat. Rev. Neurosci.* 9, 856–869. <http://dx.doi.org/10.1038/nrn2478>.
- Nee, D.E., Brown, J.W., Askren, M.K., Berman, M.G., Demiralp, E., Krawitz, A., Jonides, J., 2013. A meta-analysis of executive components of working memory. *Cereb. Cortex* 23, 264–282. <http://dx.doi.org/10.1093/cercor/bhs007>.
- Nichols, T., Brett, M., Andersson, J., Wager, T., Poline, J.-B., 2005. Valid conjunction inference with the minimum statistic. *Neuroimage* 25, 653–660. <http://dx.doi.org/10.1016/j.neuroimage.2004.12.005>.
- Nooner, K.B., Colcombe, S.J., Tobe, R.H., Mennes, M., Benedict, M.M., Moreno, A.L., Panek, L.J., Brown, S., Zavitz, S.T., Li, Q., Sikka, S., Gutman, D., Bangaru, S., Schlachter, R.T., Kamil, S.M., Anwar, A.R., Hinz, C.M., Kaplan, M.S., Rachlin, A.B., Adelsberg, S., Cheung, B., Khanuja, R., Yan, C., Craddock, C.C., Calhoun, V., Courtney, W., King, M., Wood, D., Cox, C.L., Kelly, A.M.C., Di Martino, A., Petkova, E., Reiss, P.T., Duan, N., Thomsen, D., Biswal, B., Coffey, B., Hoptman, M.J., Javitt, D.C., Pomara, N., Sidtis, J.J., Koplewicz, H.S., Castellanos, F.X., Leventhal, B.L., Milham, M.P., 2012. The NKI-Rockland sample: a model for accelerating the pace of discovery science in psychiatry. *Front. Neurosci.* 6, 152. <http://dx.doi.org/10.3389/fnins.2012.00152>.
- O'Reilly, J.X., Beckmann, C.F., Tomassini, V., Ramnani, N., Johansen-Berg, H., 2010. Distinct and overlapping functional zones in the cerebellum defined by resting state functional connectivity. *Cereb. Cortex* 20, 953–965. <http://dx.doi.org/10.1093/cercor/bhp157>.
- O'Shea, J., Johansen-Berg, H., Trief, D., Göbel, S., Rushworth, M.F.S., 2007. Functionally specific reorganization in human premotor cortex. *Neuron* 54, 479–490. <http://dx.doi.org/10.1016/j.neuron.2007.04.021>.
- Obeso, I., Cho, S.S., Antonelli, F., Houle, S., Jahanshahi, M., Ko, J.H., Strafella, A.P., 2013. Stimulation of the pre-SMA influences cerebral blood flow in frontal areas involved with inhibitory control of action. *Brain Stimul.* 6, 769–776. <http://dx.doi.org/10.1016/j.brs.2013.02.002>.
- Power, J.D., Barnes, K.A., Snyder, A.Z., Schlaggar, B.L., Petersen, S.E., 2012. Spurious but systematic correlations in functional connectivity MRI networks arise from subject motion. *Neuroimage* 59, 2142–2154. <http://dx.doi.org/10.1016/j.neuroimage.2011.10.018>.
- Reetz, K., Dogan, I., Rolfs, A., Binkofski, F., Schulz, J.B., Laird, A.R., Fox, P.T., Eickhoff, S.B., 2012. Investigating function and connectivity of morphometric findings—exemplified on cerebellar atrophy in spinocerebellar ataxia 17 (SCA17). *Neuroimage* 62, 1354–1366. <http://dx.doi.org/10.1016/j.neuroimage.2012.05.058>.
- Reid, A.T., Bzdok, D., Langner, R., Fox, P.T., Laird, A.R., Amunts, K., Eickhoff, S.B., Eickhoff, C.R., 2015. Multimodal connectivity mapping of the human left anterior and posterior lateral prefrontal cortex. *Brain Struct. Funct.* <http://dx.doi.org/10.1007/s00429-015-1060-5>.
- Robinson, J.L., Laird, A.R., Glahn, D.C., Lovallo, W.R., Fox, P.T., 2010. Metaanalytic connectivity modeling: delineating the functional connectivity of the human amygdala. *Hum. Brain Mapp.* 31, 173–184. <http://dx.doi.org/10.1002/hbm.20854>.
- Roland, P.E., Skinhøj, E., Lassen, N.A., Larsen, B., 1980. Different cortical areas in man in organization of voluntary movements in extrapersonal space. *J. Neurophysiol.* 43, 137–150.
- Rottschy, C., Langner, R., Dogan, I., Reetz, K., Laird, A.R., Schulz, J.B., Fox, P.T., Eickhoff, S.B., 2012. Modelling neural correlates of working memory: a coordinate-based meta-analysis. *Neuroimage* 60, 830–846. <http://dx.doi.org/10.1016/j.neuroimage.2011.11.050>.
- Rottschy, C., Caspers, S., Roski, C., Reetz, K., Dogan, I., Schulz, J.B., Zilles, K., Laird, A.R., Fox, P.T., Eickhoff, S.B., 2013. Differentiated parietal connectivity of frontal regions for “what” and “where” memory. *Brain Struct. Funct.* 218, 1551–1567. <http://dx.doi.org/10.1007/s00429-012-0476-4>.
- Rushworth, M.F.S., Johansen-Berg, H., Göbel, S.M., Devlin, J.T., 2003. The left parietal and premotor cortices: motor attention and selection. *Neuroimage* 20 (Suppl. 1), S89–S100.
- Satterthwaite, T.D., Elliott, M.A., Gerraty, R.T., Ruparel, K., Loughead, J., Calkins, M.E., Eickhoff, S.B., Hakonarson, H., Gur, R.C., Gur, R.E., Wolf, D.H., 2013. An improved framework for confound regression and filtering for control of motion artifact in the preprocessing of resting-state functional connectivity data. *Neuroimage* 64, 240–256. <http://dx.doi.org/10.1016/j.neuroimage.2012.08.052>.
- Schubotz, R.I., von Cramon, D.Y., 2002a. Predicting perceptual events activates corresponding motor schemes in lateral premotor cortex: an fMRI study. *Neuroimage* 15, 787–796. <http://dx.doi.org/10.1006/nimg.2001.1043>.
- Schubotz, R.I., von Cramon, D.Y., 2002b. A blueprint for target motion: fMRI reveals perceived sequential complexity to modulate premotor cortex. *Neuroimage* 16, 920–935.
- Seeley, W.W., Crawford, R.K., Zhou, J., Miller, B.L., Greicius, M.D., 2009. Neurodegenerative diseases target large-scale human brain networks. *Neuron* 62, 42–52. <http://dx.doi.org/10.1016/j.neuron.2009.03.024>.
- Segall, J.M., Allen, E.A., Jung, R.E., Erhardt, E.B., Arja, S.K., Kiehl, K., Calhoun, V.D., 2012. Correspondence between structure and function in the human brain at rest. *Front. Neuroinform.* 6, 10. <http://dx.doi.org/10.3389/fninf.2012.00010>.

- 1144 Smith, S.M., Nichols, T.E., 2009. Threshold-free cluster enhancement: addressing
1145 problems of smoothing, threshold dependence and localisation in cluster inference.
1146 *Neuroimage* 44, 83–98. <http://dx.doi.org/10.1016/j.neuroimage.2008.03.061>.
- 1147 Smith, S.M., Jenkinson, M., Woolrich, M.W., Beckmann, C.F., Behrens, T.E.J., Johansen-Berg,
1148 H., Bannister, P.R., De Luca, M., Drobnjak, I., Flitney, D.E., Niazy, R.K., Saunders, J.,
1149 Vickers, J., Zhang, Y., De Stefano, N., Brady, J.M., Matthews, P.M., 2004. Advances in
1150 functional and structural MR image analysis and implementation as FSL. *Neuroimage*
1151 23 (Suppl. 1), S208–S219. <http://dx.doi.org/10.1016/j.neuroimage.2004.07.051>.
- 1152 Stoodley, C.J., Schmahmann, J.D., 2009. Functional topography in the human cerebellum:
1153 a meta-analysis of neuroimaging studies. *Neuroimage* 44, 489–501. <http://dx.doi.org/10.1016/j.neuroimage.2008.08.039>.
- 1154 Tanji, J., Okano, K., Sato, K.C., 1988. Neuronal activity in cortical motor areas related to ip-
1155 silateral, contralateral, and bilateral digit movements of the monkey. *J. Neurophysiol.*
1156 60, 325–343.
- 1157 Thickbroom, G.W., Byrnes, M.L., Mastaglia, F.L., 2003. Dual representation of the hand in
1158 the cerebellum: activation with voluntary and passive finger movement. *Neuroimage*
1159 18, 670–674.
- 1160 Turkeltaub, P.E., Eden, G.F., Jones, K.M., Zeffiro, T.A., 2002. Meta-analysis of the functional
1161 neuroanatomy of single-word reading: method and validation. *Neuroimage* 16,
1162 765–780.
- 1163 Turkeltaub, P.E., Eickhoff, S.B., Laird, A.R., Fox, M., Wiener, M., Fox, P., 2012. Minimizing
1164 within-experiment and within-group effects in activation likelihood estimation
1165 meta-analyses. *Hum. Brain Mapp.* 33, 1–13. <http://dx.doi.org/10.1002/hbm.21186>.
- 1166 Uddin, L.Q., Kelly, A.M.C., Biswal, B.B., Margulies, D.S., Shehzad, Z., Shaw, D., Ghaffari, M.,
1167 Rotrosen, J., Adler, L.A., Castellanos, F.X., Milham, M.P., 2008. Network homogeneity
1168 reveals decreased integrity of default-mode network in ADHD. *J. Neurosci. Methods*
1169 169, 249–254. <http://dx.doi.org/10.1016/j.jneumeth.2007.11.031>.
- 1170 Vincent, J.L., Patel, G.H., Fox, M.D., Snyder, A.Z., Baker, J.T., Van Essen, D.C., Zempel, J.M.,
1171 Snyder, L.H., Corbetta, M., Raichle, M.E., 2007. Intrinsic functional architecture in
1172 the anaesthetized monkey brain. *Nature* 447, 83–86. <http://dx.doi.org/10.1038/nature05758>.
- 1173
1174
- Ward, N.S., Frackowiak, R.S.J., 2003. Age-related changes in the neural correlates of motor
1175 performance. *Brain* 126, 873–888. 1176
- Weinrich, M., Wise, S.P., 1982. The premotor cortex of the monkey. *J. Neurosci.* 2, 1177
1329–1345. 1178
- Wise, S.P., Murray, E.A., 2000. Arbitrary associations between antecedents and actions.
1179 *Trends Neurosci.* 23, 271–276. 1180
- Wise, S.P., Boussaoud, D., Johnson, P.B., Caminiti, R., 1997. Premotor and parietal cortex:
1181 corticocortical connectivity and combinatorial computations. *Annu. Rev. Neurosci.*
1182 20, 25–42. <http://dx.doi.org/10.1146/annurev.neuro.20.1.25>. 1183
- Wymbs, N.F., Grafton, S.T., 2013. Contributions from the left PMd and the SMA during
1184 sequence retrieval as determined by depth of training. *Exp. Brain Res.* 224, 49–58. 1185
<http://dx.doi.org/10.1007/s00221-012-3287-1>. 1186
- Yeo, B.T.T., Krienen, F.M., Sepulcre, J., Sabuncu, M.R., Lashkari, D., Hollinshead, M.,
1187 Roffman, J.L., Smoller, J.W., Zöllei, L., Polimeni, J.R., Fischl, B., Liu, H., Buckner, R.L.,
1188 2011. The organization of the human cerebral cortex estimated by intrinsic functional
1189 connectivity. *J. Neurophysiol.* 106, 1125–1165. <http://dx.doi.org/10.1152/jn.00338.2011>. 1190
1191
- Zhang, X., de Beukelaar, T.T., Possel, J., Olaerts, M., Swinnen, S.P., Woolley, D.G., Wenderoth,
1192 N., 2011. Movement observation improves early consolidation of motor memory. 1193
J. Neurosci. 31, 11515–11520. <http://dx.doi.org/10.1523/JNEUROSCI.6759-10.2011>. 1194
- Zhu, F., Yeung, A., Poolton, J., Lee, T., Leung, G., Masters, R., 2015. Cathodal transcranial
1195 direct current stimulation over left dorsolateral prefrontal cortex area promotes
1196 implicit motor learning in a golf putting task. *Brain Stimul.* <http://dx.doi.org/10.1016/j.brs.2015.02.005>. 1197
1198
- Zielinski, B.A., Gennatas, E.D., Zhou, J., Seeley, W.W., 2010. Network-level structural
1199 covariance in the developing brain. *Proc. Natl. Acad. Sci. U. S. A.* 107, 18191–18196. 1200
<http://dx.doi.org/10.1073/pnas.1003109107>. 1201
- zu Eulenburg, P., Caspers, S., Roski, C., Eickhoff, S.B., 2012. Meta-analytical definition
1202 and functional connectivity of the human vestibular cortex. *Neuroimage* 60, 162–169. 1203
<http://dx.doi.org/10.1016/j.neuroimage.2011.12.032>. 1204